Geological Magazine

www.cambridge.org/geo

A high-resolution palynological and geochemical study of the end-Triassic mass-extinction based on a new cored succession at Winterswijk (the Netherlands)

Remco Bos[1], Roel-Jan van Zonneveld[1], Jelle W.F. Reumer[1,2,3], Geert-Jan Vis[4], Nico Janssen[4], Teun Everwijn[1], Appy Sluijs[1] and Bas van de Schootbrugge[1]

[1]Department of Earth Sciences, Faculty of Geosciences, Utrecht University, Princetonlaan 8, 3584 CB Utrecht, the Netherlands; [2]Natural History Museum Rotterdam, P.O. Box 23452, NL-3001 KL Rotterdam, the Netherlands; [3]Naturalis Biodiversity Center, Darwinweg 2, 2333 CR Leiden, the Netherlands and [4]TNO - Geological Survey of the Netherlands, Princetonlaan 6, 3508 TA Utrecht, the Netherlands

Original Article

Cite this article: Bos R, van Zonneveld R-J, Reumer JWF, Vis G-J, Janssen N, Everwijn T, Sluijs A, and van de Schootbrugge B. A high-resolution palynological and geochemical study of the end-Triassic mass-extinction based on a new cored succession at Winterswijk (the Netherlands). *Geological Magazine* **161**(e17): 1–19. https://doi.org/10.1017/S0016756824000323

Received: 29 February 2024
Revised: 26 September 2024
Accepted: 3 October 2024

Keywords:
terrestrial palynology; vegetation disturbance; Central Atlantic Magmatic Province; climate variability; end-Triassic crisis

Corresponding author:
Remco Bos; Email: r.bos@uu.nl

Abstract

Based on a new cored succession at Winterswijk, evidence is uncovered of the end-Triassic mass-extinction (ETME) event in a subsurface sedimentary succession of the Netherlands. The ETME was one of the most devastating events for the biosphere during the Phanerozoic era. Massive volcanism from the Central Atlantic Magmatic Province initiated the breakup of the supercontinent Pangea and resulted in terrestrial and marine extinction pulses, which drastically altered the course of life on Earth. The newly cored material reveals a sedimentary succession representing a shallow marine setting dominated by laminated black shale and claystone deposits. A high-resolution palynostratigraphic dataset provides evidence for a late Rhaetian vegetation assemblage that displays a stepwise decline of arborescent tree vegetation that is transiently replaced by a community of ferns and fern allies. Geochemical records link this major disturbance in palynofloral biodiversity to a pulse of volcanic activity as evidenced by a negative excursion in stable organic carbon isotopes. Shifts towards drier climate conditions, as inferred from sedimentary elemental composition, suggest continental aridification strongly influenced the terrestrial realm following volcanic pulses. Presence of reworked material suggests unstable soils that were affected by increased erosion rates, inhibiting the re-establishment of conifer tree vegetation. Comparison of our findings with other contemporaneous European Triassic-Jurassic boundary sections confirms the progression of the end-Triassic extinction, which exhibits a two-phased structure. The presence of the ETME in the subsurface of the Netherlands provides further evidence towards our understanding of terrestrial extinction with emphasis on the decline of vegetation.

1. Introduction

The Winterswijk quarry in the eastern Netherlands is a unique location that exposes Triassic sediments close to the surface. Based on palynological assessments, a middle Triassic, Anisian age was determined for the carbonate sequences (Visscher and Commissaris, 1968) of the 'Muschelkalk'. Later on, Lower Jurassic and Cenozoic deposits overlying the Muschelkalk were also recognized, cropping out in areas around the Winterswijk quarry (Harsveldt, 1973; van den Bosch *et al.* 1975; Herngreen *et al.* 2005). Subsequent quarry expansion has revealed a peculiar ~11 metre succession of black shale and red claystone deposits overlying the Muschelkalk in the northern flank of Quarry IV (Fig. 1). Preliminary palynological data strongly hinted at a late Rhaetian age, which was confirmed by magnetostratigraphy (van Hinsbergen *et al.* 2019) and findings of a diverse assemblage of Rhaetian shark teeth (de Lange *et al.* 2023). Here, we investigate whether Rhaetian successions in Winterswijk also contain a record of the end-Triassic mass-extinction (ETME) event.

The ETME has not been documented in the strata of the subsurface of the Netherlands, but its detection could provide significant insight into the progression of major extinction patterns in a key location in the Central European Basin (CEB) (Fig. 2). The ETME (~201.5 Ma) is often causally linked to volcanic activity of the Central Atlantic Magmatic Province (CAMP) initiating the breakup of the supercontinent of Pangea (Deenen *et al.* 2010; Blackburn *et al.* 2013; Percival *et al.* 2017; Landwehrs *et al.* 2020; Ruhl *et al.* 2020). CAMP-flood basalt emissions are generally held responsible for the extensive dieback in the marine/terrestrial biosphere through climate warming/cooling, acid rain and marine anoxia. An estimated release of 8,000 Gt to 100,000 Gt of

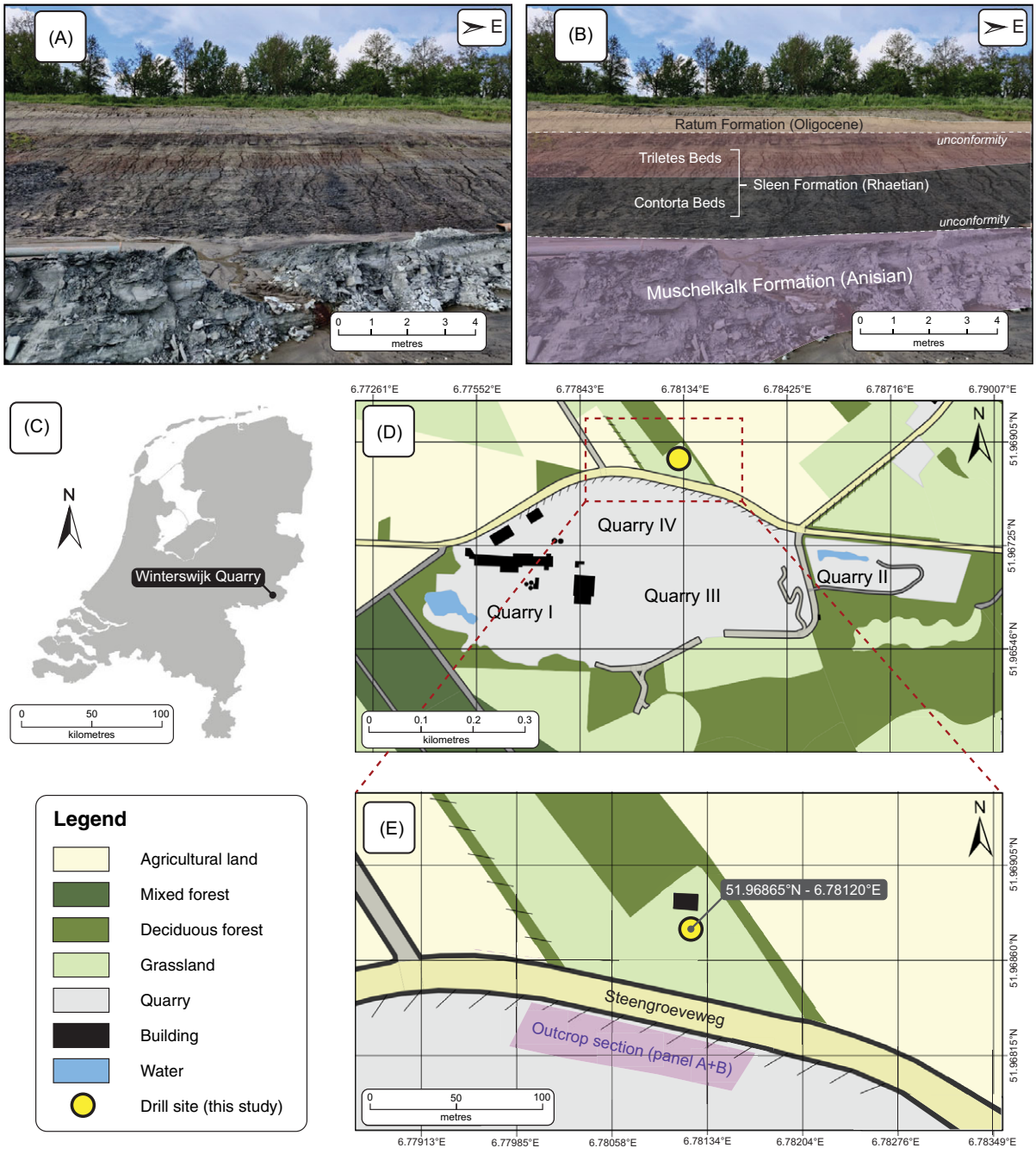

Figure 1. (A) Outcrop section on the north side of the Winterswijk Quarry with (B) subdivisions of Triassic and Cenozoic stratigraphic sections. (C) Map of the Netherlands indicating position of the Winterswijk Quarry. (D+E) Schematic map of the Winterswijk Quarry indicating position of the drill location and outcrop section.

CO_2 (Beerling and Berner, 2002; Heimdal *et al.* 2018; Capriolo *et al.* 2022) resulted in highly elevated atmospheric pCO_2 (Steinthorsdottir *et al.* 2011) and caused a rise in global temperature between 3 and 6°C (McElwain *et al.* 1999; Huynh and Poulsen, 2005). Several climate archives record at least a doubling of atmospheric pCO_2 to nearly 5000 ppm during the earliest Jurassic (Schaller *et al.* 2011; Schaller, 2012). Coupled ocean-atmosphere climate models demonstrate that significantly increased pCO_2 forcing causes continental aridification and enhanced seasonality in coastal regions of the Pangean landmasses (Huynh and Poulsen, 2005; Landwehrs *et al.* 2020; Landwehrs *et al.* 2022). In addition, acid rain, frequent wildfires and increasing weathering/erosion rates are factors that contributed to the instability of terrestrial and marine biomes (van de Schootbrugge *et al.* 2020; Bos *et al.* 2023).

Recent analyses of marine and terrestrial records revealed a two-phased extinction (Gravendyck *et al.* 2020; Wignall and Atkinson, 2020; Lindström, 2021; Bos *et al.* 2023). Episodes of increased extinction rates and ecosystem disturbance coincide with two negative excursions in stable carbon isotopic composition ($\delta^{13}C$) of the global exogenic carbon pool, as reflected in sedimentary organic carbon. This revealed that pulsed CAMP-emissions influenced the global exogenic carbon pool and the biosphere (Hesselbo *et al.* 2002; Deenen *et al.* 2010; Ruhl *et al.*

https://doi.org/10.1017/S0016756824000323

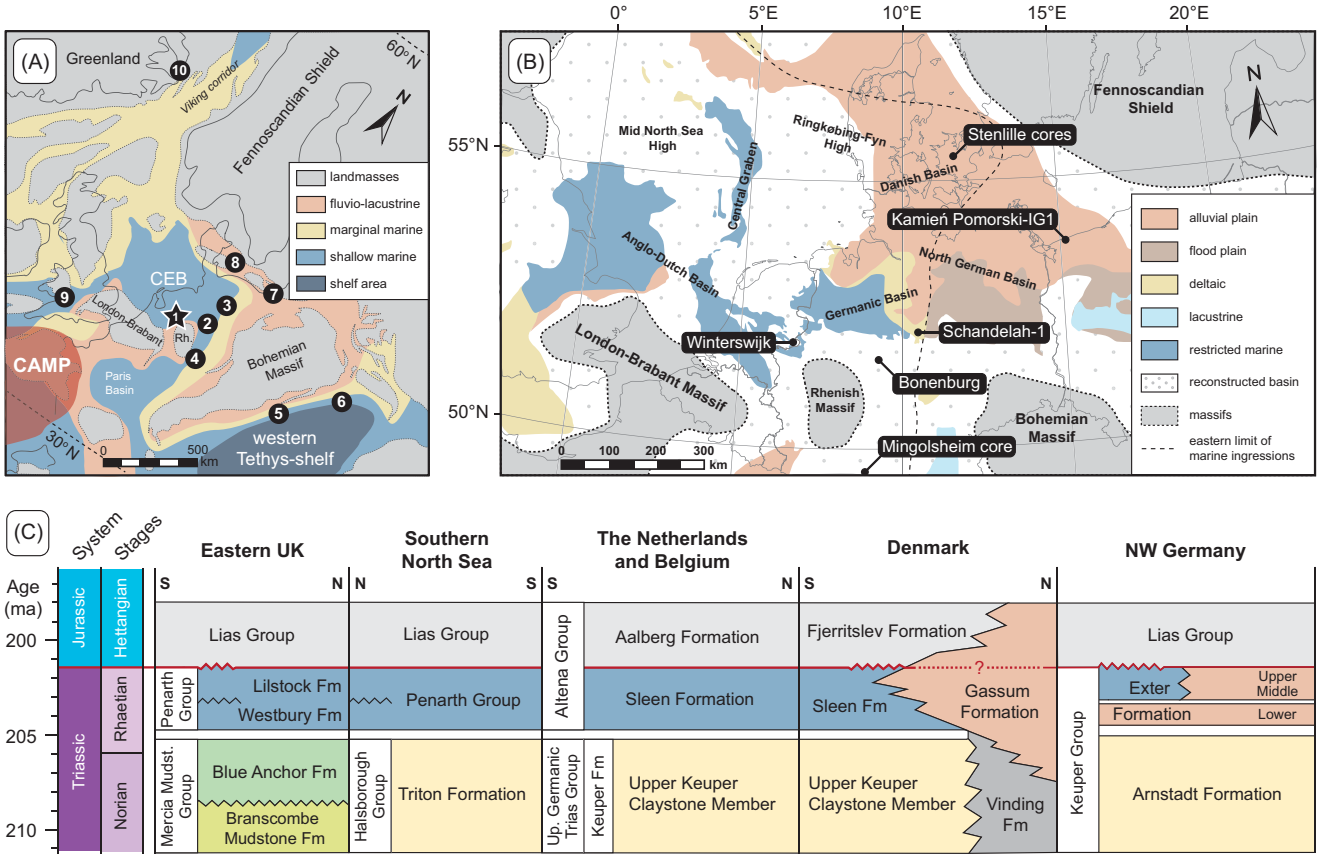

Figure 2. (A) Palaeogeographic reconstruction depicting depositional regime of NW Europe and positions of Triassic-Jurassic boundary sections (black circles) that reported terrestrial palynological records. Modified after Blakey (2014). 1) Star indicates the position of the newly drilled Winterswijk core. Contemporary sections include 2) Bonenburg (Germany, Gravendyck et al. (2020)), 3) Schandelah-1 (Germany, Bos et al. (2023)), 4) Mingolsheim (Germany, van de Schootbrugge et al. (2009)), 5) Kuhjoch (Austria, (Bonis *et al.* 2009; von Hillebrandt *et al.* 2013)), 6) Csővár section (Hungary; Götz et al. (2009)), 7) Kamień Promorski-IG1 (Poland; Pieńkowski et al. (2012)) 8) Stenlille (Denmark, Lindström et al. (2012)), 9) St. Audrie's Bay (UK, (Bonis *et al.* 2010; Bonis and Kürschner, 2012) and 10) Astarekløft (East Greenland; Mander et al. (2013)). (B) Present-day distribution and facies of Upper Triassic (Rhaetian) strata in NW Europe. Modified after Doornenbal and Stevenson (2010) (Chapter 9). Position of the Winterswijk drill core and other key palynostratigraphic sections are noted. (C) Triassic correlation chart with red line indicating the base of the Lower Jurassic. The colours of the formations correspond to the sediment facies of panel B. Modified after Doornenbal and Stevenson (2010) (Chapter 9).

2010a; Whiteside *et al.* 2010; Lindström *et al.* 2012; Corso *et al.* 2014; Hesselbo *et al.* 2023). Elevated sedimentary mercury (Hg) concentrations provide evidence that links these negative CIEs to volcanic activity (Thibodeau *et al.* 2016; Percival *et al.* 2017; Kovács *et al.* 2020). The onset of the ETME is linked to a first pulse, which resulted in a stepwise decline in arborescent conifers (Lindström, 2021; Bos *et al.* 2023) and thus vacated open landscapes that were gradually colonized by pioneering spore-producing ferns/fern allies (Ruckwied *et al.* 2008; Götz *et al.* 2009; Larsson, 2009; van de Schootbrugge *et al.* 2009; Schneebeli-Hermann *et al.* 2017; van Konijnenburg-van Cittert *et al.* 2020; van Konijnenburg-van Cittert *et al.* 2021; van Konijnenburg-van Cittert *et al.* 2022). This interlude period of fern dominance is generally expressed through a so-called 'fern spike' and is referred to as the main disturbance interval for terrestrial and marine ecosystems with little to no extinctions being reported (Larsson, 2009; van de Schootbrugge *et al.* 2009; Wignall and Atkinson, 2020; Lindström, 2021; Bos *et al.* 2023). This disturbance interval culminates into the second phase of the ETME with the true extinction of Triassic tree taxa at the Triassic-Jurassic boundary (Lindström, 2021). The extinction of Triassic vegetation resulted in major turnovers in dominant plant biomes (McGhee *et al.* 2013; Lindström, 2016) establishing Early Jurassic vegetation and a significant component of present-day flora (Rees *et al.* 2000). However, uncertainties still remain in the magnitude of this turnover (Barbacka *et al.* 2017) and the potential causes.

We investigate a recently drilled core from Upper Triassic marginal marine sediments near Winterswijk (the Netherlands) and provide the first evidence for the presence of the ETME in subsurface of the Netherlands based on a detailed palynostratigraphic framework of this new section. Based on palynofloral assemblages, we employ standard diversity indices (richness, evenness, dominance and the Shannon-Wiener index) to assess the impact of the ETME on plant ecosystems. Additionally, we use sediment geochemistry to reconstruct palaeo-environmental and palaeo-climate conditions. This study puts particular emphasis on the transition from pre-extinction conditions to extinction interval from an ecological perspective and aims to evaluate patterns in floral changes at the onset of the ETME.

2. Regional palaeogeography and stratigraphic framework

The palaeogeographic setting of the Winterswijk depositional site is in the south of the CEB (Fig. 2A). During Late Triassic/Early Jurassic times, northwestern Europe was characterized by high sea levels relative to the modern (van der Meer *et al.* 2022) resulting in

https://doi.org/10.1017/S0016756824000323

an epicontinental seaway with isolated small landmasses (Manspeizer, 1994; Golonka *et al.* 2018). The European Epicontinental Seaway was situated at mid-latitudes (30–50°N) dominated by marginal fluvio-lacustrine and shallow marine depositional settings (Fig. 2). Notable landmasses surrounded the CEB, including the Rhenish Massif to the south, London-Brabant Massif to the southwest, the Bohemian Massif to the east and the Fennoscandian Shield to the north. The CEB lies in a proximate position to major volcanic activity of the northern extents of CAMP volcanism, which reached up to Iberia and western France (Caroff and Cotten, 2004) (Fig. 2A). Sediment distribution indicates restricted marine facies in the southwest of the CEB from several sub-basins such as the Anglo-Dutch and Germanic Basin (Fig. 2B). Towards the northeast of the CEB, the sedimentary facies transitions to deltaic and fluvial deposits, which dominate the North German and Danish Basins. The Winterswijk core is situated at the western edges of the Germanic Basin and is mainly represented by the restricted marine facies of the Sleen Formation, which has been dated to the Rhaetian (van Hinsbergen *et al.* 2019; de Lange *et al.* 2023). This formation is equivalent to the marine Rhaetian deposits of the Penarth Group (Westbury Fm and Lilstock Fm) from the UK and southern North Sea (Fig. 2C). The Rhaetian fluvial facies of northern Germany and Denmark are represented by the Exter Formation and Gassum Formation, respectively. Marine deposits are not uncommon in the Rhaetian sections of Denmark and Germany, which indicates roughly the extent of marine ingression on the eastern side of the CEB (Fig. 2C).

Stratigraphic correlations of Triassic-Jurassic boundary sections have been conducted using $\delta^{13}C_{TOC}$ records that show two distinct negative stable carbon isotope excursions (CIEs), reflecting the volcanic injection of ^{13}C-depleted carbon (Hesselbo *et al.* 2002; Deenen *et al.* 2010; Ruhl *et al.* 2010b; Whiteside *et al.* 2010; Lindström *et al.* 2012; Corso *et al.* 2014). These are known as the Marshi ('precursor') and Spelae ('initial') CIEs and can be widely traced (Lindström *et al.* 2017). The volcanic origin of these excursions has been substantiated using sedimentary Hg-enrichments (Percival *et al.* 2017; Kovács *et al.* 2020; Percival *et al.* 2021) as well as Hg-isotope signatures (Yager *et al.* 2021; Shen *et al.* 2022a; Shen *et al.* 2022b; Bos *et al.* 2024). Furthermore, Upper Rhaetian chronostratigraphy is mainly recognized by occurrences of marine fossil groups such as ammonites, bivalves, echinoderms, brachiopods and conodonts. Ammonites have been widely used as biostratigraphic markers to correlate sections across the CEB. Based on the global stratotype sections and point (GSSP) site at Kuhjoch, the last occurrence (LO) of the ammonite *Choristoceras marshi* is recognized to mark the onset of the ETME across Europe (von Hillebrandt *et al.* 2013), while the base of the Jurassic is defined by the first occurrence of the ammonite *Psiloceras spelae tirolicum* (von Hillebrandt *et al.* 2007; von Hillebrandt and Krystyn, 2009; von Hillebrandt *et al.* 2013). These ammonite bioevents are closely associated with the two main negative CIEs (Lindström *et al.* 2017).

Based on palynofloral records, the co-occurrence of the fern spore *Polypodiisporites polymicroforatus* and the pollen taxon *Ricciisporites tuberculatus* provides evidence for the main disturbed interval of the ETME across European sites (Lindström *et al.* 2017), including the GSSP section at Kuhjoch (Bonis *et al.* 2009). In addition, the occurrence of a 'fern spike' is widely recognized across the North German Basin (Lindström *et al.* 2017), which largely consists of *P. polymicroforatus* spores (van de Schootbrugge *et al.* 2009). In contrast, the abundance of *R. tuberculatus* shows more spatial variability. The fern spike interval also marks the LO of several Triassic palynofloral taxa including *Rhaetipollis germanicus, Lunatisporites rhaeticus*, *R. tuberculatus* and *Ovalipollis ovalis*. The top of the fern spike interval corresponds to the Spelae CIE and sees the disappearance of Triassic palynofloral taxa. In addition, this interval sees the first occurrence of the accessory marker pollen taxon *Cerebropollenites thiergartii*, marking the base of the Early Jurassic (Hettangian), which is synonymous with the first occurrence (FO) of *P. spelae* in stratigraphic successions at the GSSP section in the Eiberg Basin (Kuerschner *et al.* 2007). Aquatic palynomorphs indicate similar biostratigraphic correlative potential, most notably by the last common occurrence (LCO) of the dinoflagellate species *Rhaetogonyaulax rhaetica* (Bonis *et al.* 2010; Li *et al.* 2016; Lindström *et al.* 2017; Peng *et al.* 2018; Gravendyck *et al.* 2020).

3. Material and Methods

3. a. Scientific drilling and sample collection

The drilling operation was conducted during May and June of 2021 in the Dutch province of Gelderland, close to the town of Winterswijk yielding a 25.90-metre core (Fig. 1; GPS coordinates: 51.96865°N – 6.78120°E). The resulting borehole is registered by the Geological Survey of the Netherlands (TNO) under borehole number B41F0262. The drill site has an elevation of 41.79 metres above local reference level (NAP) and forms part of the Winterswijk Quarry site managed by Sibelco B.V. Early explorations of the upper strata in the quarry revealed Rhaetian aged sediments capping the well-known 'Muschelkalk' of Anisian age (Visscher and Commissaris, 1968), dipping approximately 10° to the north (Fig. 1A+B). The drill site location was therefore determined just north of the quarry in a small meadow (Fig. 1D+E). The drilling activities were performed by Thijssen Drilling Company B.V. (Geulle, the Netherlands) using a Nordmeyer DSB-1. Clean water was used as drilling fluid for the first 15 metres using an auger drill due to the unconsolidated nature of the layers. The remainder of the core (15 – 25.9 metres) was drilled with a diamond bit upon reaching more indurated strata. A casing was introduced to provide stability to the borehole and prevent the upper layers from collapsing inward. The 1-metre core sections with a diameter of 100 mm were placed in storage boxes and transported to the Earth Simulation Laboratory at Utrecht University (Supplementary Fig. S1), where they were stored in a cooling cell at ~4 °C. The studied interval (Rhaetian section = ~11 metres) of the core was sampled with 2 cm resolution and placed in plastic sampling bags for storage.

3. b. Gamma ray well-logging

After completion of the drilling operations, well-logging was carried out using a multitool measuring probe by the commercial company Metinco B.V., which was lowered at a constant rate (1 metre/min) down the borehole. The gamma ray logging, as measured on potassium, uranium and thorium, results in a distinctive overview of the natural gamma radiation emitted by the lithologic units. The top ~14.5 metres of the borehole was fitted with a metallic casing, which resulted in a weaker gamma ray signal. The overall implementation of logging is completed with the use of a SCOUT Pro Data Acquisition System and the data processing is achieved with WELLCAT™ software. The quality of the data acquisition is considered to be good for the entire section without any anomalies. The gamma ray signature provides an

https://doi.org/10.1017/S0016756824000323

overall image of the lithology of the substrate surrounding the borehole. Lower intensity values reflect a low clay content and/or high silica content, whereas higher intensities reflect high clay content and/or low silica content. The presence of glauconite will also result in high radiation intensity and higher gamma ray signal.

3. c. Palynology

A total of 55 samples were processed for palynology with an average resolution of ~20 cm within the studied interval. All samples were oven-dried and approximately 5–7 g of material was crushed. Samples were subsequently supplemented with a *Lycopodium* tablet for absolute quantification and subjected to a standard palynological protocol at Utrecht University. This procedure involves a single treatment with 10% HCl solution for the removal of carbonates and dissolution of the *Lycopodium* tablet and double treatment with 38% HF (hydrofluoric acid) for the removal of siliciclastic elements. Treatments of 30% HCl were performed after every HF processing step to prevent the precipitation of CaF_2. Residual material was sieved using a 10 µm nylon-mesh, homogenized and permanently mounted using a combination of 5% Polyvinyl Alcohol solution and glue on glass slides. Counting of 200 – 300 palynomorphs per sample was conducted using light microscopy (400x magnification). One sample (19.825 mbs) yielded too little palynomorphs and was counted to 150 specimens. Terrestrial palynological (i.e. spores and pollen grains from land plants) records are presented as relative abundances (%) of the total palynofloral assemblage. Palynomorph species were determined using photographic references from previously well-studied sections (Heunisch *et al.* 2010; Gravendyck *et al.* 2020; Bos *et al.* 2023; Lindström *et al.* 2023).

To assess palynofloral diversity, we calculate a number of statistical diversity indices that include species richness (S; number of species), Shannon-Wiener index (H), Simpson index of Dominance and Pielou's Evenness. The Shannon-Wiener index (Shannon and Weaver, 1949) represents $H = -\Sigma p_i * \ln(p_i)$, where p_i is the proportion of species i (n_i/n), implying it is a function of relative abundances and the number of taxa. Simpson index of Dominance is calculated as the sum of p_i squared (dominance = $\Sigma(p_i^2)$) and notes the disproportionate commonness of particular taxa (Simpson, 1949). The conceptual inverse of dominance is called (Pielou's) evenness (= e^(H/S)), which normalizes species richness. PAST 3 software was used to compute these indices (Hammer *et al.* 2001). The Shannon-Wiener index (diversity), evenness and dominance are calculated based on the total palynofloral assemblage excluding aquatic and non-pollen palynomorphs. Varying sample sizes could affect the amplitudes of the diversity indices. However, all samples yielded enough palynomorphs (200 – 300 specimens) with a single exception (19.825 mbs).

3. d. Magnetic susceptibility

A total of 194 samples were analyzed for magnetic susceptibility (MS) with an average resolution of ~5 cm in the studied interval. Initially, the mass of the bulk sample and of the 40 ml plastic vials containing the selected samples was determined. The measurements were performed at room temperature using a AGICO MFK1-FA device at the palaeomagnetic laboratory (Fort Hoofddijk) at Utrecht University. Each sample was measured three times to correct for environmental and temperature-based influences and to assess the short-term reproducibility and variability, showing an average relative standard deviation of 0.2%. To account for drift within a single run, duplicates were introduced to determine the long-term reproducibility. Basic bulk MS settings were conducted using a standard frequency of 976 Hz with a weak variable magnetic field of 200 A/m. Results were corrected for the total weight of the sample. We present the raw measurements supplemented with a 4-point moving average to assess the long-term trends in the record. High MS intensities are generally interpreted to represent terrestrial weathering inputs (siliclastics), while lower intensities can result from high fractions of organic matter and/or carbonates (Warrier and Shankar, 2009).

3. e. TOC and bulk organic carbon isotopes

Organic carbon concentration and stable isotope ratios were determined for 114 samples covering the upper Rhaetian interval of the Winterswijk core with an average resolution of ~8 cm. All samples were oven-dried, powdered and treated twice using 10% HCl and rinsed with de-ionized water for the removal of carbonates (inorganic carbon), after which residues were homogenized and analyzed for organic carbon content using a Carbon, Nitrogen, Sulphur (CNS) analyser (NA 1500) at Utrecht University. The total organic carbon (TOC) content was calculated by multiplying the measured carbon content with ratio of the decarbonated and original sample weights. The precision in TOC determinations is 0.7%. Samples were subsequently analyzed for $\delta^{13}C_{TOC}$ using a Fisons 1500 CNS Elemental Analyzer coupled to a Finnigan MAT Delta Plus mass spectrometer, bracketed by an in-house standard (Granite-Quartzite, value: -26.86‰ Vienna Pee Dee Belemnite (VPDB), determined using IAEA standards). Accuracy and precision comprise 0.03‰ and 0.01‰ for the $\delta^{13}C_{TOC}$ measurements, respectively, and are reported relative to the VPDB.

3. f. ICP-OES elemental analysis

Using Inductively Coupled Plasma – Optical Emission Spectrometry (ICP-OES; Perkin Elmer Avio 500) at Utrecht University, quantitative elemental composition was determined on a total of 88 samples with an average resolution of ~8 cm. Oven-dried and powdered sedimentary rock (100–125 mg) was subjected to total destruction using 2.5 ml HF and 2.5 ml $HClO_4$ /HNO_3 (2:3) mixture in a closed Teflon container and stored on a 90 °C hot plate overnight. Samples were heated to 140 °C and subsequently re-dissolved in 1M HNO_3 at 90 °C during a second night. A residual solution of ~6 ml was transferred to 15 ml Greiner tubes for analysis. The average overall accuracy (recovery) was between 97 and 108% and based on in-house standards, duplicates and an internal Germanium standard, an average analytical uncertainty of 1% was determined.

Certain trace elements enriched in fine-grained shale, such as Sr, Ba, Cu, Ti, V, Cr, Ni and Co, can reveal paleoclimate and palaeo-redox conditions (Meng *et al.* 2012; Bai *et al.* 2015; Fu *et al.* 2016; Moradi *et al.* 2016; Borrok *et al.* 2019). Particularly, redox-sensitive elements, such as V, Cr, Ni and Co, are widely used with the ratios of V/Cr and Ni/Co considered to be reliable palaeo-redox indicators. Higher ratios correspond to a decrease in oxygen levels for both proxies. The reconstruction of the palaeo-salinity and paleoclimate conditions is derived from the ratios of Sr/Ba and Sr/Cu (Moradi *et al.* 2016).

https://doi.org/10.1017/S0016756824000323

4. Results

4. a. Core description and lithological indicators

The Winterswijk drilling project yielded a 25.90 m succession (supplementary Fig. S1) encompassing several distinct stratigraphic units that have been previously described and assigned to the Middle Triassic (Anisian; Muschelkalk Fm; Visscher and Commissaris (1968)) and Late Triassic (Rhaetian; Sleen Fm; van Hinsbergen et al. (2019)), Oligocene (Ratum Fm–Winterswijk Fm; van den Bosch et al. (1975)), Miocene-Pliocene (Brinkheurne Fm–Miste Beds; van den Bosch et al. (1975)) and Quaternary (Fig. 3). The lowermost unit (25.90 – 24.04 mbs) consists of heavily bioturbated laminated grey/white limestone known as the 'Muschelkalk'. These deposits are of Anisian age (Visscher and Commissaris, 1968). The uppermost 10 cm (24.18 – 24.08) of this unit consists of a grey marl with alternating dark/light grey layering, containing silt and burrows.

A sharp lithological transition is noted at 24.08 mbs (Supplementary Fig. S1). The Muschelkalk is overlain by finely laminated black shales (Contorta Beds) containing bivalve remains (*Rhaetavicula contorta*) (diameter = ~2 cm; 24.08 – 20.17 mbs), which, in turn, transitions sharply to red/greyish clays (20.17 – 13.53 mbs; Triletes Beds) (Fig. 3). These two units have been previously dated to represent the late Rhaetian (van Hinsbergen *et al.* 2019; de Lange *et al.* 2023). A ~2 cm thick pyritic layer is present at 21.70 mbs. Several horizons within the laminated shale interval exhibit pyritized bivalve remains. A further subdivision can be made for the bottom part of the red claystone interval (20.17 – 18.24 mbs), which consists of dark grey claystone interbedded with brown-red claystone containing plant and coal remains. A number of grey claystone beds can be discerned that are interbedded within the red claystone succession. No macrofossils were found within the upper part of the red claystone unit (18.24 – 13.53 mbs). This unit containing laminated shales and reddish claystone beds is reminiscent of the upper Rhaetian sections in the Germanic Basin with the shale-dominated Contorta Beds transitioning to the red-brown claystone interval of the Triletes Beds (Gravendyck *et al.* 2020). These two units will be referred to as Contorta and Triletes Beds and belong to the Sleen Formation (Fm), which is the equivalent of the Exter Formation in Germany (Fig. 2C). Further correlative efforts have revealed that the Sleen Fm corresponds to the Penarth Group (Westbury and Lilstock Fms) in the UK (Doornenbal and Stevenson, 2010).

A second unconformity is recognized at the top of the red claystone interval (13.53 mbs), where the claystone is sharply overlain by clay-rich sands with glauconite-containing beds (13.53 – 11.65 mbs). This lithological unit corresponds to the Ratum Formation, which commonly overlays Mesozoic deposits across the larger Winterswijk area and has been suggested to be of Oligocene (early Rupelian) age (van den Bosch *et al.* 1975; Herngreen *et al.* 2005). This unit transitions to several metres of a fine to medium sand unit (11.65 – 8.00 mbs) with minimal clay content and weak layering. This section is consistent with the Winterswijk Formation (van den Bosch *et al.* 1975; Herngreen *et al.* 2005) with indications of late Rupelian age. The interval between 8.00 mbs and 5.00 mbs shows facies with a distinctly higher fraction of greyish/brown clay. This interval corresponds to the Brinkheurne Formation of Miocene age and is overlain by the Miste Beds (5.00 – 2.00 mbs) of Miocene-Pliocene age, consisting of silt to fine sands with olive-green hue of colour (van den Bosch *et al.* 1975). The upper two metres of the core consists of grey to orange/brown fine sands with traces of topsoil, likely derived from Quaternary (glacial) deposits. The core description is summarized in Supplementary Table S1.

The gamma ray signature of the lowermost limestone unit (Muschelkalk) shows moderate intensity that sharply increases at the upper marl bed at 24.18 mbs (Fig. 3), likely denoting a higher clay content. The lower part of the Rhaetian section (Contorta Beds, 24.08 – 20.17 mbs) shows roughly double the intensity of the underlying limestone unit, which continues into the lower section of the Triletes Beds (20.17 – 13.53 mbs) with minimal internal variability, which likely reflects the continuously high fraction of finer clays (and absence of carbonates). There is a notable peak at the lowermost bed of the Triletes Beds (20.17 – 20.00 mbs). The upper part of the Triletes Beds exhibits a notable drop of gamma ray intensity to values similar to the Muschelkalk, presumably representing a change in the clay content. The internal variability of the Triletes Beds is similar compared to the Contorta Beds. The upper 13.53 m shows the lowest gamma ray intensity with the previously defined stratigraphy indicating a distinct signature based on the amount of clay and/or glauconite presence. Sandy units tend to show lower gamma ray intensity, while higher clay/glauconite content is noted by relatively higher intensities. The gamma ray intensities of the Winterswijk core are summarized in Supplementary Table S2.

The sedimentary composition of the upper Rhaetian deposits of the Winterswijk core is inferred from measurements of MS, which provides insight into the major sedimentary components, such as siliciclastics/clays (weathering products), organic matter and carbonates. MS intensities indicate a clear separation between the Contorta Beds and Triletes Beds. The MS intensity is the lowest in the Contorta Beds with minimal variation and displays a sharp 5-fold increase across the transition interval (T1-T3) to the Triletes Beds (20.15 mbs), which rapidly returns to lower values at the top of this transition (19.58 mbs, T3). A gradual increase in MS intensity is observed for the upper interval of the Triletes Beds (19.58 – 14.45 mbs), roughly doubling that of the Contorta Beds and showing more substantial variation. A notable drop is noted in the uppermost interval (14.45 – 13.53 mbs). Magnetic susceptibility measurements are summarized in Supplementary Table S4.

4. b. Palynofloral biostratigraphy

Palynological assessment of the presumed late Rhaetian deposits (24.08 – 13.56 mbs) revealed the presence of several distinct Late Triassic taxa and assemblages that confirm a late Rhaetian age (Fig. 4). The *Rhaetipollis-Limbosporites* (RLi) zone is distinguished by low abundances (2 – 10%) of *R. germanicus* and very low abundances (0–2%) of *Limbosporites lundbladii*. This palynofloral zone is generally synonymous with the Contorta Beds (24.08 – 20.17 mbs) and is marked by the occurrence of several typical late Rhaetian pollen-taxa, such as *O. ovalis* (1– 10%), *L. rhaeticus* (0–5%), *R. tuberculatus* (5 – 10%) and *Alisporites sp.* (0 – 3%), while spore-taxa such as *Zebrasporites* ssp. (0 – 1%) and *P. polymicroforatus* (0 – 2%) are less common (Plate I and II). The RLi zone is widely used for correlation across Europe (Lund, 1977; Kuerschner *et al.* 2007; Bonis *et al.* 2009; Lindström *et al.* 2017; Gravendyck *et al.* 2020). Overall, the Contorta Beds of Winterswijk are characterized by a pollen-dominated assemblage with high abundances of the cheirolepid conifers (*Classopollis* sp., ~50%) and the gymnosperm *R. tuberculatus* (~10%), and the periodic influx of dinoflagellate cysts (*R. rhaetica* and *Dapcodinium priscum*, see Supplementary Table S6). An overall biome that is rich in upper canopy tree vegetation is inferred from additional abundances of

https://doi.org/10.1017/S0016756824000323

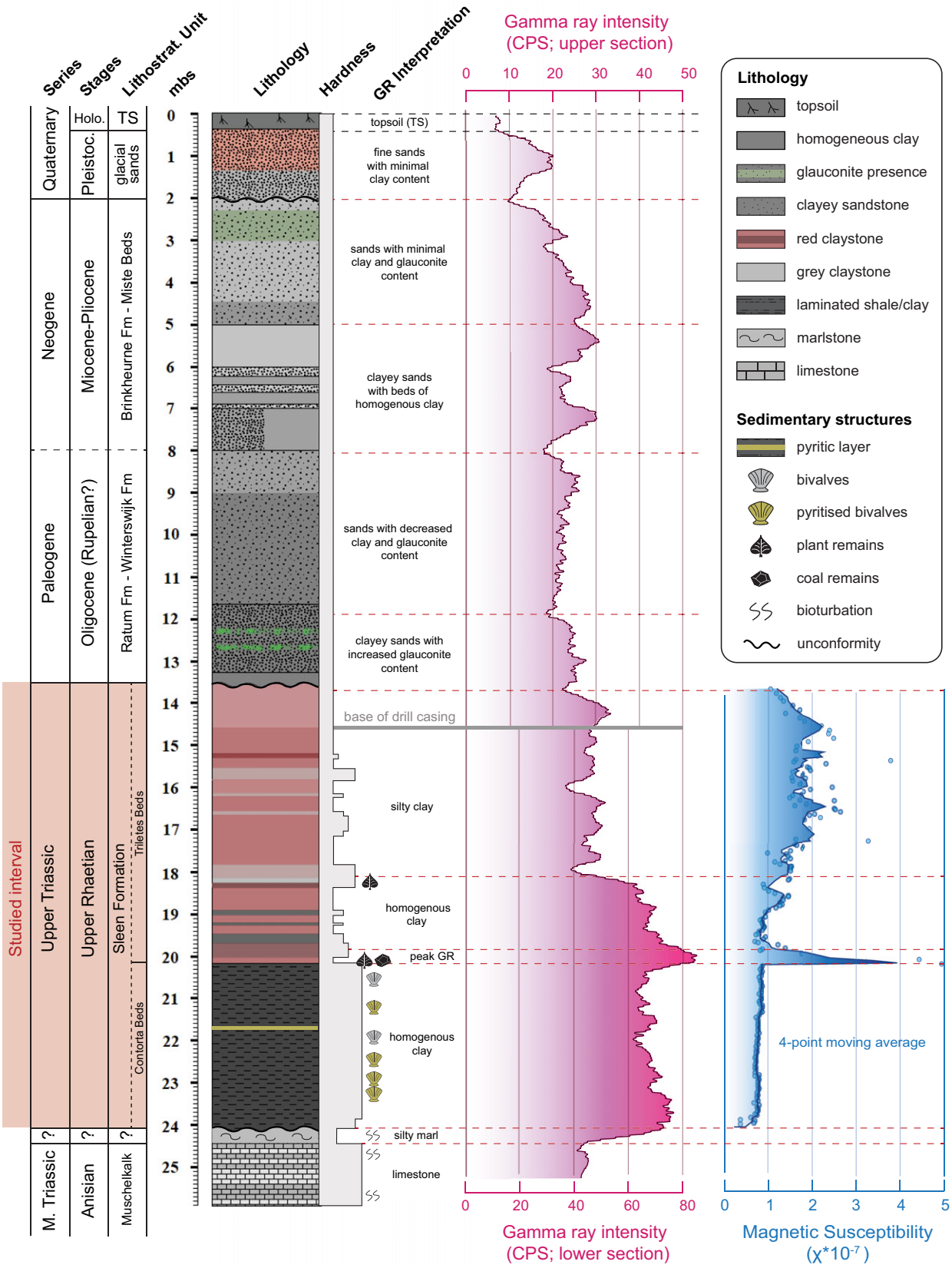

Figure 3. Stratigraphic column of Winterswijk core section depicting (left panel) formations, stratigraphic units and lithology. The middle panel shows the gamma ray intensity from borehole logging. Note different scale for the upper 14.5 metres due to the borehole casing causing lower intensities. Magnetic susceptibility intensity is plotted on the right side with a 4-point moving average.

https://doi.org/10.1017/S0016756824000323

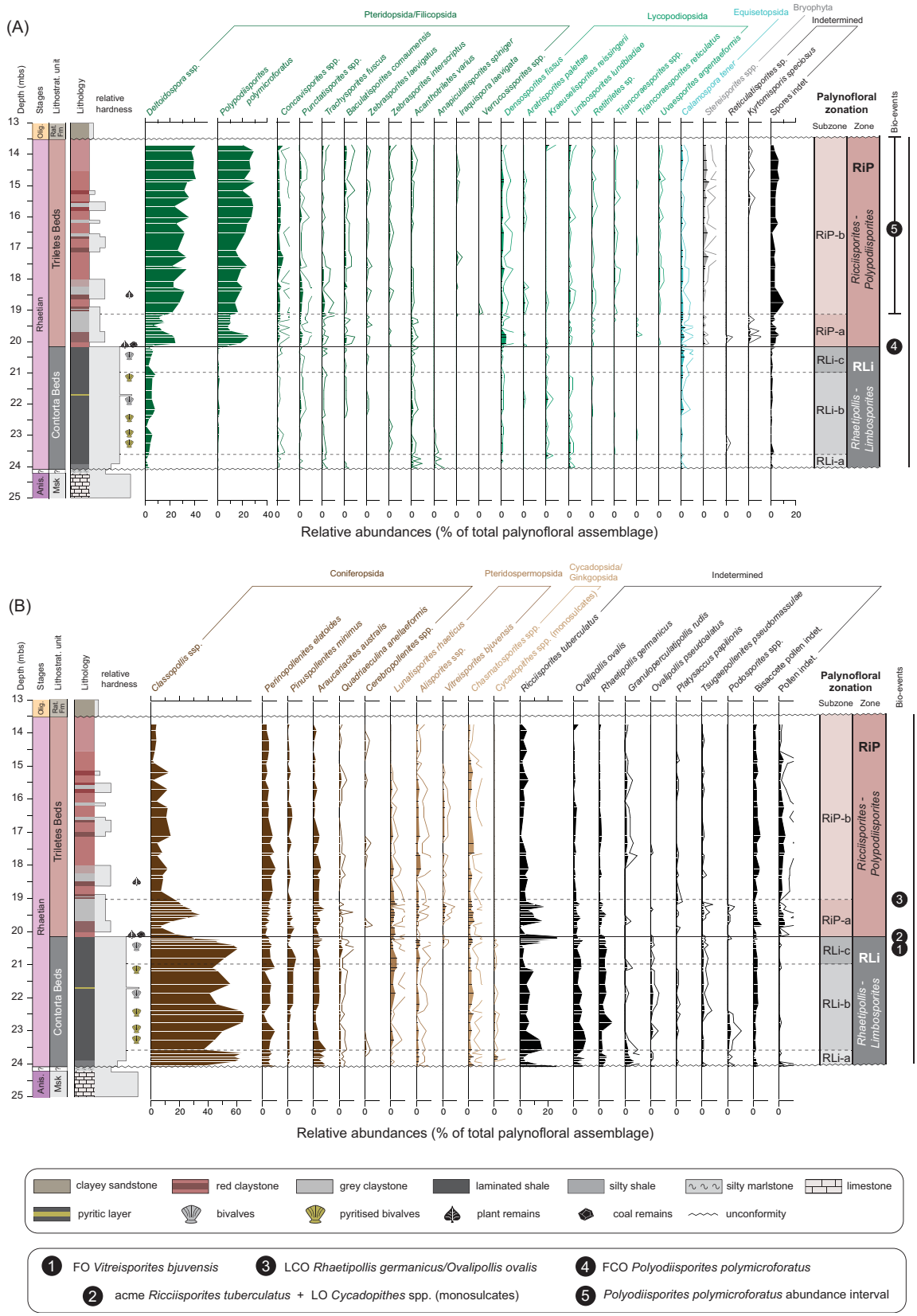

Figure 4. Relative abundances of palynofloral species in the research interval of the Winterswijk core depicting significant occurrences of spore-taxa (A) and pollen-taxa (B). Palynofloral assemblage zones were determined by visual grouping of important marker species and bio-events: RLi = *Rhaetipollis-Limbosporites*, RiP = *Ricciisporites-Polypodiisporites*. Horizontal lines indicate position of boundaries of several palynofloral assemblage (sub)zones. Marker species bio-events denote the position of last occurrences, last common occurrences, first occurrences, first common occurrences and acmes. Solid lines in graphs represent 4 times exaggeration of the relative abundance.

https://doi.org/10.1017/S0016756824000323

taxodiaceous conifers (*Perinopollenites elatoides*), the pollen-taxa of *O. ovalis* and various types of bisaccate pollen. Nearly all spore-producing taxa show minimal occupancy of the ground vegetation during deposition of the Contorta Beds with the exception of ground/tree ferns (*Deltoidospora* sp.) and horsetails (*Calamospora tener),* which are consistently present. Furthermore, four periodic increases of pollen assigned to the family Coniferopsida (most notably cheirolepid conifers of *Classopollis* sp.) are observed throughout the Contorta Beds, while other types of vegetation display minimal variation.

The RLi zone of the Winterswijk core can be further subdivided into three subzones (Fig. 4). The lowermost of these subdivisions (RLi-a; 24.08 – 23.22 mbs) is characterized by peak abundances of *R. tuberculatus* (~25%), *Classopollis* ssp. (~70%) and *Granuloperculatipollis rudis* (~6.3%). The RLi-b subzone (23.22 – 20.74 mbs) is characterized by the consistently low abundance of *R. germanicus*, *O. ovalis*, *R. tuberculatus* and *Classopollis* ssp. with minimal variation. Lastly, the upper section of the Contorta Beds in Winterswijk (20.74 – 20.17 mbs) is denoted by the RLi-c subzone and shows a notable high abundance of *Classopollis* ssp. (~62%) and a higher abundance of the horsetail-derived spore species *C. tener* (~3%). Another notable feature of this interval is the apparent drop in abundance of *R. tuberculatus* (<2%), which shows a sudden resurgence at the top of the RLi-c zone to about 15% of the palynofloral assemblage. The FO of the bisaccate pollen *Vitreisporites bjuvensis* also occurs within this interval.

A number of aquatic palynomorph taxa similarly denote the late Rhaetian age of the Winterswijk core. In particular, relatively high abundances (of the total assemblage) of the Rhaetian dinoflagellate cyst species *R. rhaetica* and *D. priscum* are noted for the RLi-a (~3%) and RLi-C (~4%) subzones, while the intermediated RLi-b subzone shows more moderate abundances (~1%) with minimal variation. In addition, minor occurrences of the dinoflagellate cyst *Lunnomidinium* sp. (<0.5% of total assemblage) are noted for the RLi-c subzone.

The transition to the overlying Triletes Beds is marked by the first common occurrence of *P. polymicroforatus* (10 – 30%) and other morphotypes of *Concavisporites-Deltoidospora* (10 – 40%), culminating in a 'fern spike interval' (Larsson, 2009; van de Schootbrugge *et al.* 2009) or *P. polymicroforatus* abundance interval (Fig. 4) (Lindström, 2016; Lindström *et al.* 2017). The co-occurrence with *R. tuberculatus* is denoted as the RiP (*Ricciisporites-Polypodiisporites*) palynological zone and can be used to stratigraphically correlate the Late Triassic crisis among records across NW Europe (Larsson, 2009; van de Schootbrugge *et al.* 2009; Lindström, 2016; Lindström *et al.* 2017; Gravendyck *et al.* 2020; Bos *et al.* 2023). Furthermore, the RiP palynological zone is considered to be the main disturbance interval of the terrestrial and marine ETME in the CEB (Lindström *et al.* 2017). The entire assemblage of the Triletes Beds shifts to a spore-dominated assemblage mainly represented by pteridopsid ferns (*P. polymicroforatus*, *Concavisporites* spp. and *D. mesozoica*) (~60%) and a group of isoetalean lycopods (*Densosporites fissus*). A synchronous increase in horsetails (*C. tener*) and mosses (*Stereisporites* sp.) is noted as well for the Triletes Beds. Most pollen-taxa seem unaffected in their relative abundances after the transition to the Triletes Beds, except for *Classopollis* sp., which diminishes to about 10%. This trend is also reflected in the absolute palynomorphs amounts (Fig. 7), which shows overall high concentrations (>10^5 palynomorphs/gram sediment) in the Contorta Beds with periodic increases corresponding to increased abundances of *Classopollis* sp. Pollen concentrations drop to much lower concentration (<10^4 palynomorphs/gram sediment) at 20.17 mbs and remain low for the entirety of the Triletes Beds.

The Triletes Beds are subdivided into RiP-a in the lower part (20.17 – 19.11 mbs) and RiP-b for the upper part (19.11 – 13.53 mbs). RiP-a subzone is characterized by an acme in *R. tuberculatus* in the lowermost section (20.15 mbs) that was initiated on the top part of RLi-c subzone (20.25 mbs). This acme is closely followed by a sharp increase in *P. polymicroforatus* (~20%) and morphotypes of *Concavisporites-Deltoidospora* (~20%) between 20.03 mbs and 19.53 mbs after which these spore-taxa diminish and are replaced by *R. tuberculatus* (~17%). In addition, the top of the RiP-a subzone marks the LCO of both *O. ovalis* and *R. germanicus* (19.53 mbs). Finally, a relatively high abundance of dinoflagellate cysts *R. rhaetica* and *D. priscum* (~10% of total assemblage) is noted for the top of RiP-a subzone (19.19 mbs), which mark the LCO of both species. The remainder of the Triletes Beds (RiP-b subzone) is distinguished by relatively high abundances of reworked palynomorphs (2 – 8% of the total assemblage) that include Paleozoic acritarchs (Plate I) (van de Schootbrugge *et al.* 2020) and Anisian spores (Plate I) (Brugman *et al.* 1985). All palynological data are summarized in Supplementary Table S6.

4. c. Organic carbon content and $\delta^{13}C_{TOC}$

The $\delta^{13}C_{TOC}$ signature of the Rhaetian deposits of the Winterswijk core can clearly be separated in two distinct intervals with average values of -27.0‰ in the Contorta Beds and values averaging -24.8‰ in the overlying Triletes Beds, with a sharp ~2‰ positive excursion at 20.17 mbs. Consistently, TOC values average 3.44% in the Contorta Beds and sharply decrease at 20.17 mbs to an average of 0.42% in the Triletes Beds. Within the top of the Contorta Beds, $\delta^{13}C_{TOC}$ values show a trend towards lower values, which is mirrored in the TOC values. Several negative $\delta^{13}C_{TOC}$ excursions can be recognized within the Contorta Beds that correspond to periodic increases in TOC (Fig. 5). The most significant of these occur in the lowermost interval (23.51 mbs) with a magnitude of ~2.2‰ and a short-lived negative peak at -28.5‰. Three more modest negative excursions occur at 22.78 – 22.35 mbs, 21.63 – 21.43 mbs and between 20.85 – 20.17 mbs with a magnitude of about 0.5‰. The uppermost of these has been recognized as the Marshi CIE in line with the palynofloral assemblages (RLi-c subzone) and correlation with the nearby Bonenberg site in Germany (Fig. 6) (Gravendyck *et al.* 2020). This marks the transition into the Triletes Beds and is subdivided into three intervals (T1 – T3; Fig. 5). Following the positive excursion at the transition into Triletes Beds (20.17 mbs), $\delta^{13}C_{TOC}$ values remain high between 20.15 mbs and 19.745 mbs (T2) after which a modest negative excursion (magnitude = ~1.1‰) between 19.61 mbs and 19.11 mbs is noted (T3) peaking to -25.8‰, which is accompanied with a minimal increase in TOC (0.66%). The remainder of the Triletes Beds (19.11 – 13.53 mbs) shows minimal variation. All TOC and $\delta^{13}C_{TOC}$ values are reported in Supplementary Table S3.

4. d. Elemental chemistry

Elemental composition is derived from ICP-OES elemental analysis (Supplementary Table S5), which provides further insights into climatic and redox conditions. The ratio of V/Cr shows an average of 1.25 in the shales of the Contorta Beds (24.08 – 20.17 mbs), with a distinct peak (~1.4) between 22.78 – 22.35 mbs, corresponding to a peak in TOC and moderate negative CIE (Fig. 5). A similar signature is noted for the Ni/Co with an average of 3.32, with overall Ni/Co values correlating with TOC ($R^2 = 0.65$) and V/Cr to a lesser degree ($R^2 = 0.27$; Supplementary Figure S2).

https://doi.org/10.1017/S0016756824000323

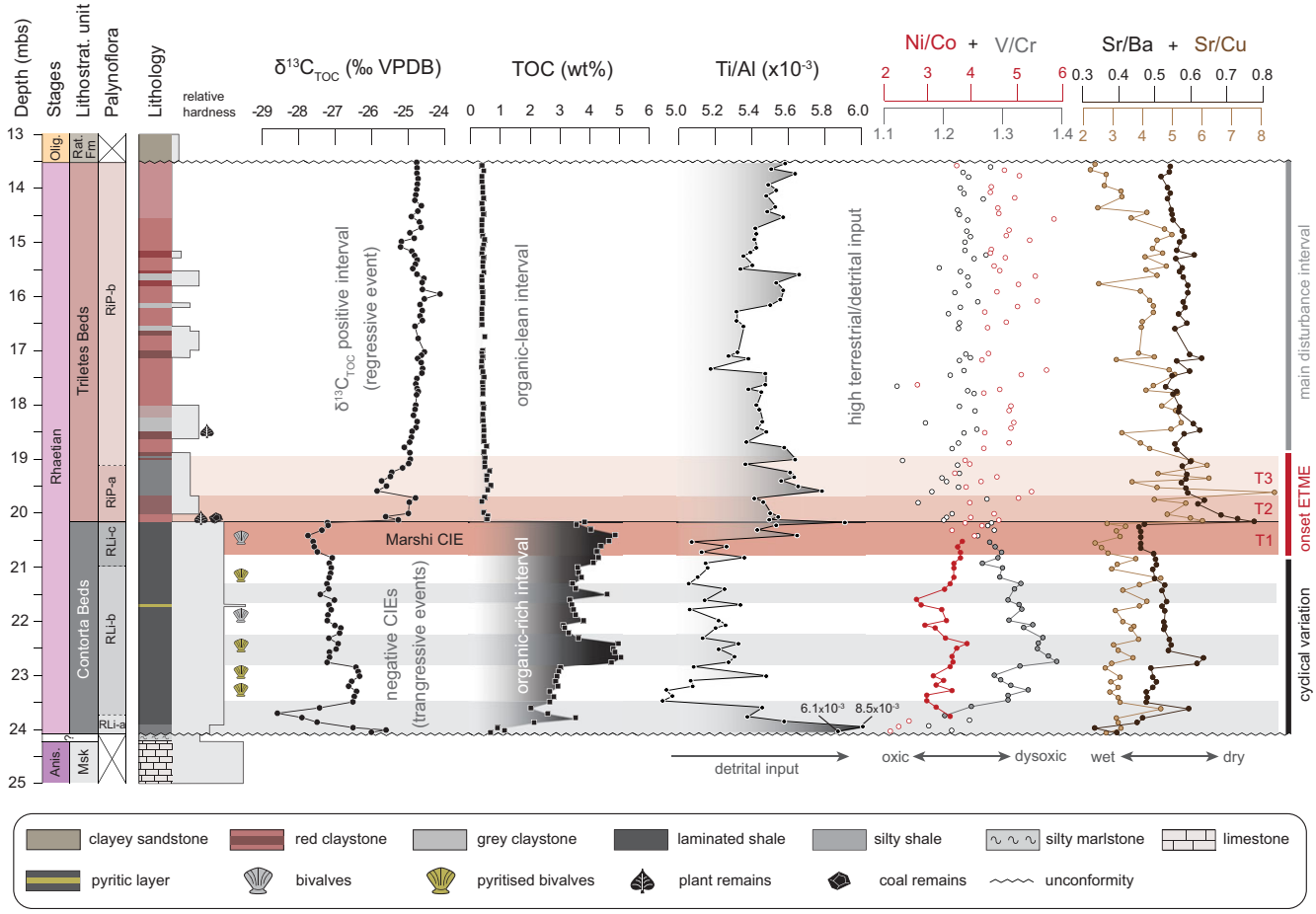

Figure 5. Geochemical measurements of the studied interval of the Winterswijk core showing bulk organic carbon isotope record (Vienna Peedee Belemnite) and total organic carbon concentrations. Elemental analysis is depicted for terrestrial input (Ti/Al), redox variation (V/Cr and Ni/Co) and precipitation (Sr/Ba and Sr/Cu).

The V/Cr ratio decreases to an average of 1.1 in the Triletes Beds, while the Ni/Co increases to an average of 4.6 in the same interval. This discrepancy is likely caused by detrital input, which is well-known to affect palaeo-redox indicators (Rimmer, 2004). Ti/Al ratios are relatively low in the Contorta Beds (average = 0.051) indicative of low detrital input (Chen *et al.* 2013). An increase in Ti/Al is observed for the uppermost interval of the Contorta Beds (20.44 – 20.17 mbs, T1) and values remain high in the Triletes Beds (average = 0.055) indicating higher detrital input. Therefore, we consider the palaeo-redox indicators (V/Cr and Ni/Co) to be inconclusive for the red claystone-dominated interval of the Triletes Beds. The Sr/Ba ratios vary between 0.4 and 0.6 (average = 0.52) in the Contorta Beds and increase to an average of 0.6 in the Triletes Beds. The Sr/Ba ratio correlates weakly with MS ($R^2 = 0.42$) with a peak (0.84) between 20.17 mbs and 19.745 mbs (T2). A decrease to an average value of 0.62 is noted for the T3 interval. The Sr/Cu ratios of shales from the Contorta Beds vary between 2 and 4 (average = 3.3). An increase in noted for the T2 interval and peaks within the T3 interval (8.3). The average Sr/Cu value for the remainder of the Triletes Beds is 4.4.

5. Discussion

5. a. Stratigraphic correlations

The lithology of the studied interval of the Winterswijk section is strongly reminiscent of the deposits of the Bonenburg section (Schobben *et al.* 2019; Gravendyck *et al.* 2020). The lower unit of the Contorta Beds in the Bonenburg succession consists of an organic-rich mudstone (shale) facies that is sharply overlain by a silt-rich (reddish) mudstone facies of the Triletes Beds. In German sections, these units belong to the Exter Fm, which is equivalent to the Sleen Formation in Winterswijk. Furthermore, the transition between the Contorta and Triletes Beds marks a broader sedimentological shift that usually is paired with a regressive interval across the CEB with high siliciclastic input and less negative $\delta^{13}C_{TOC}$ values in various T-J boundary sections (Bonis *et al.* 2009; van de Schootbrugge *et al.* 2009; Pieńkowski *et al.* 2012; Lindström *et al.* 2017; Gravendyck *et al.* 2020; Bos *et al.* 2023; Lindström *et al.* 2023). The contact between the Muschelkalk Fm and Sleen Fm of Winterswijk is characterized by an unconformity. Elevated occurrences of reworked palynomorphs in the Triletes Beds, including specimens that resemble Anisian-derived spores (Brugman *et al.* 1985), hint that the Muschelkalk was exposed during the late Rhaetian and was partly eroded. The absence of any reworked palynomorphs in the Contorta Beds also suggests higher sea-levels during deposition compared to the Triletes Beds. The nature of the unconformity at the top of the studied interval remains uncertain with nearly ~160 million years missing. The reddish colour of the Triletes Beds could indicate post-depositional oxidation due to (sub)areal exposure, suggesting an erosional surface at this horizon. Although Early Jurassic strata are not exposed at the Winterswijk quarry, several studies have described

https://doi.org/10.1017/S0016756824000323

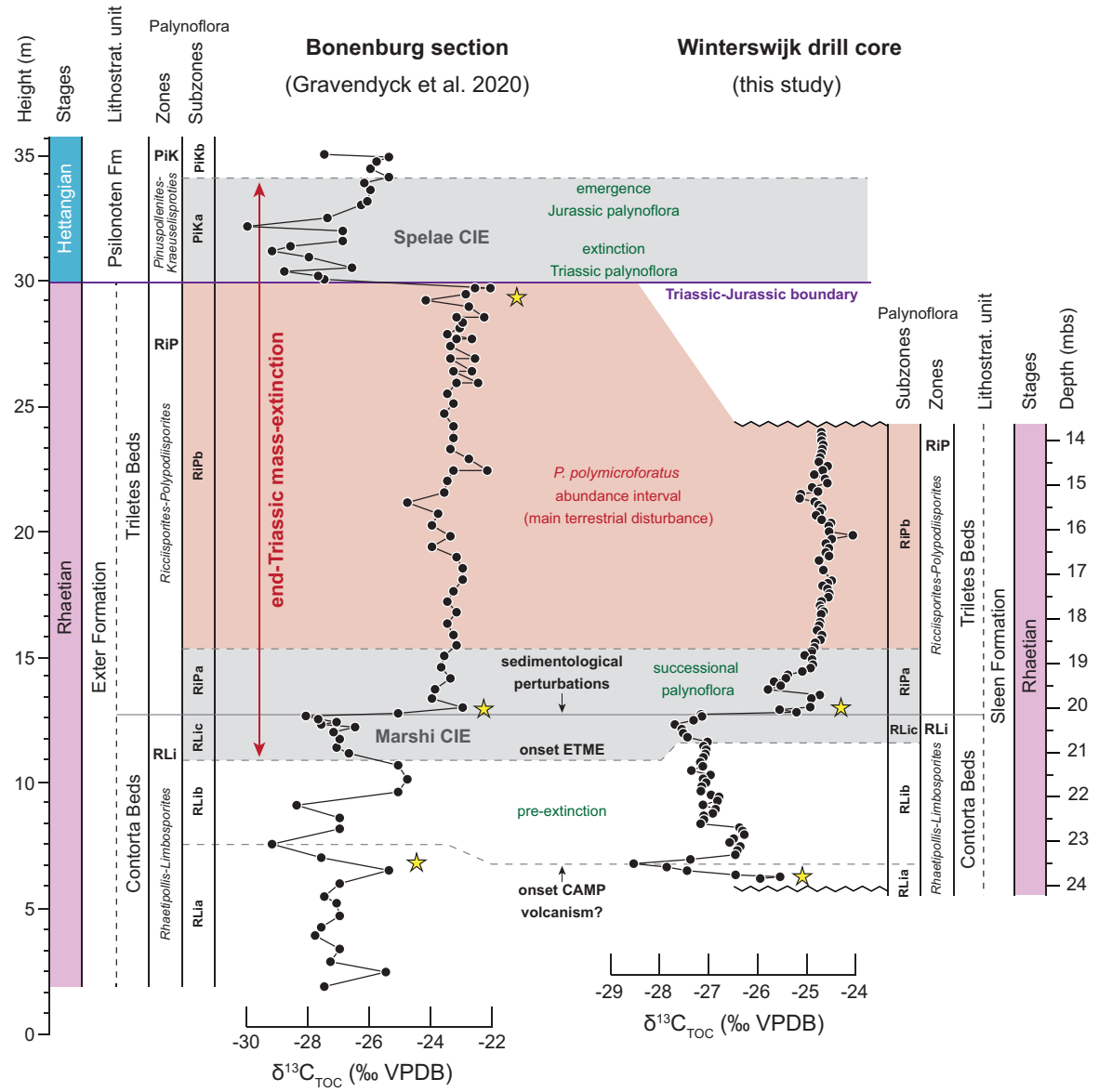

Figure 6. Correlation of organic carbon isotope records of the Bonenburg section (Gravendyck *et al.* 2020) and the Winterswijk section (this study). The yellow stars indicate the position of palynofloral disturbance in both sections.

the contact of the Sleen Fm with Lower Jurassic units (Aalburg Fm; Fig. 2C) in the surrounding area (van den Bosch *et al.* 1975; Herngreen *et al.* 2005; van Hinsbergen *et al.* 2019). The Triletes Beds facies of the upper Sleen Fm in the Winterswijk core and quarry outcrop seems to be restricted to the immediate surrounding area with no other recorded descriptions.

The co-occurrence and abundances of Late Triassic palynofloral species *P. polymicroforatus* and *R. tuberculatus* (RiP palynofloral zone) are diagnostic for the presence of the end-Triassic mass-extinction (ETME) within the subsurface of the Netherlands. This transition marks the onset of the ETME and is traceable through palynofloral changes and corresponds to the Marshi CIE (van de Schootbrugge *et al.* 2009; Gravendyck *et al.* 2020; van de Schootbrugge *et al.* 2020; Bos *et al.* 2023). Commonly, a decrease in arborescent conifers and other upper canopy tree vegetation is noted within the transition interval with a stepwise increase in ferns and fern allies occupying the vacated niches (van de Schootbrugge *et al.* 2009; Bonis and Kürschner, 2012; Lindström, 2016; Lindström *et al.* 2017; Gravendyck *et al.* 2020; Bos *et al.* 2023). The Bonenburg section displays a similar pre-extinction dominance of *Classopollis*-producing conifers with a stepwise decline at the onset of the ETME (Gravendyck *et al.* 2020). This trend is also noted in the St. Audrie's Bay section in the UK (Bonis *et al.* 2009), Mingolsheim in southern Germany (van de Schootbrugge *et al.* 2009), and several well-studied sites on the southside of the Bohemian Massif, including the Kuhjoch Global Stratotype Section and Point (GSSP) site (Bonis *et al.* 2009) from the Eiberg Basin and the Csővár section on the western Tethys shelf (Götz *et al.* 2009). In contrast, eastern sections of the CEB represented by Schandelah (Bos *et al.* 2023), Stenlille (Lindström *et al.* 2023) and Kamień Pomorski-IG1 (Pieńkowski *et al.* 2012) show a much lower relative abundance of *Classopollis*-producing conifers, instead showing higher occurrences of the mire-adapted conifers that produced *P. elatoides*. This distribution of dominant conifer types suggests the presence of a vegetation and/or climate gradient dividing the CEB between a southwestern and a

https://doi.org/10.1017/S0016756824000323

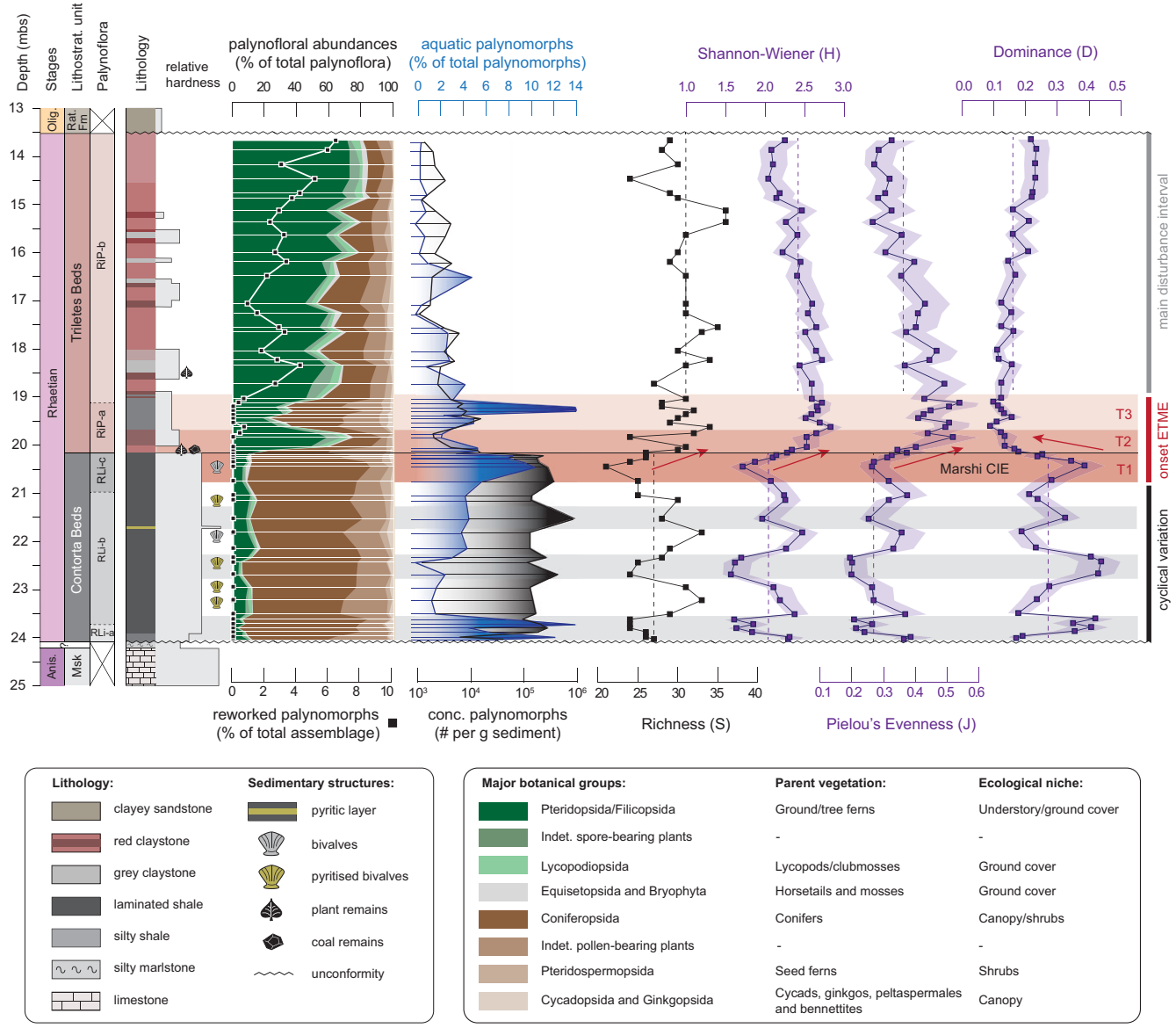

Figure 7. Palynofloral diversity indices are presented with the variation of major botanical groups, parent vegetation and ecological niches. The relative abundance of reworked palynomorphs is presented with the white line and black square data points. Species richness (black squares), Pielou's evenness, dominance and Shannon-Wiener Index (diversity) (purple squares) are given for terrestrial palynomorphs excluding aquatic, reworked and other palynomorphs. The purple-shaded area indicates the lower and upper limits of indices. The median value for each index is indicated by a red dotted vertical line and separately calculated for each interval (Contorta Beds and Triletes Beds) excluding the transition interval. Absolute palynomorphs abundances and the relative abundance of aquatic palynomorphs are presented as well. Horizontal grey bars indicate intervals of environmental and palynofloral changes in the Contorta Beds, while the red horizontal bars show the onset of the end-Triassic mass-extinction subdivided into three distinct intervals (T1-T3).

northeastern region. These biomes can be separated by vegetation that prefers cool/warm temperate (*P. elatoides*-dominated) and winter-wet conditions resembling Mediterranean areas (*Classopollis*-dominated) (Rees *et al.* 2000).

Our palynological examination within the transition interval of the Winterswijk core (T1- T3) revealed a particular structure to this reorganization in vegetation. The interval is synonymous with the RiP-a subzone and is followed by an interval that is dominant in spore-bearing vegetation (fern spike, ~80%) for the remainder of the Triletes Beds (RiP-b subzone). The spread of a pioneering fern vegetation transiently replacing gymnosperm forests has been documented from numerous sites (Fowell and Olsen, 1993; Olsen *et al.* 2002; Larsson, 2009; van de Schootbrugge *et al.* 2009). This fern-dominant interval is widely traceable and is also characterized by an increase in abundance of reworked palynomorphs (Gravendyck *et al.* 2020; van de Schootbrugge *et al.* 2020; Bos *et al.* 2023; Lindström *et al.* 2023) suggestive of widespread erosion around the CEB. A darkening of palynomorphs is also noted in the RiP-b subzone most notably in spore specimens and to a lesser degree in the pollen assemblage. This 'dark zone' was also noted in other T-J boundary sections (Lund, 2003; van de Schootbrugge *et al.* 2009). The second major extinction pulse is recorded close to the Triassic-Jurassic Boundary, corresponding to the Spelae CIE. General patterns display another biodiversity crisis within the palynoflora with several Triassic taxa going extinct (Wignall and Atkinson, 2020; Lindström, 2021). The emergence of several Early

https://doi.org/10.1017/S0016756824000323

Jurassic pollen-taxa is also noted in this interval (Bonis *et al.* 2009). This interval is unfortunately missing in the Winterswijk section due to an unconformity.

The position of the Marshi CIE is found within the Winterswijk record, which marks the onset of major volcanic activity (Hesselbo *et al.* 2002; Heimdal *et al.* 2018; Lindström *et al.* 2021). Similarly, changes in lithology are also widely recognized at the Marshi CIE around the CEB, suggestive of severe changes in regional climate conditions affecting sedimentation. The stable organic carbon isotope record from the Winterswijk core shows a signature that can be subdivided into several parts (Fig. 6). Interestingly, these subdivisions correspond to palynofloral zones, which were independently defined. Comparison with the Bonenburg section reveals a similar pattern in the $\delta^{13}C_{TOC}$ signature and the palynofloral zonation, suggesting a regional progression of the ETME (Fig. 6). The lowermost section of the Winterswijk core shows a negative CIE that corresponds to the RLi-a palynofloral subzone. This can be confidently correlated to a similar negative CIE in the Contorta Beds of the Bonenburg section, which similarly displays a subzone in the palynofloral assemblage (RLi-a) (Gravendyck *et al.* 2020). While this earlier CIE has a higher magnitude and could potentially be regarded as the Marshi CIE, the relation with palynofloral subzones does not line up with other records (Lindström *et al.* 2017).

The top of the RLi-a interval in the Winterswijk section is marked by an increase in aquatic palynomorphs, which is not as clearly expressed in the Bonenburg section. This increase hints that the negative excursions found in both sections could reflect a transgression (Schobben *et al.* 2019). This would ultimately shift the sourcing of organic matter and cause a CIE in shallow marine records. Lastly, the transition between the RLi zone (Contorta Beds; pre-extinction) and the RiP zone (Triletes Beds; main disturbance of the ETME) is marked by a positive excursion in $\delta^{13}C_{TOC}$ values in many sites across Europe (Götz *et al.* 2009; Pieńkowski *et al.* 2012; Gravendyck *et al.* 2020; Lindström, 2021; Bos *et al.* 2023; Lindström *et al.* 2023). A widespread shift in lithology indicates a substantial alteration of the depositional environment in the CEB and is mirrored by a stepwise decline in arborescent tree vegetation. This horizon is often marked by mass-rarity in many pollen-bearing taxa (Gravendyck *et al.* 2020; Lindström, 2021; Bos *et al.* 2023) and is traceable up to high latitudes on east Greenland (Mander, 2011). Whether the transition from Contorta to Triletes Beds is marked by an unconformity is uncertain. Although sharp shifts in palynological, Sr/Ba, Sr/Cu and MS data between the Contorta and Triletes Beds hint at a major drop in sedimentary rate, the palynofloral assemblages zones seem complete when compared with the nearby Bonenburg section (Gravendyck *et al.* 2020). This study did not report evidence for an unconformity at this level and therefore seems unlikely to have occurred in the Winterswijk section.

5. b. Regional ecosystem and climate variability

Prior to the onset of the ETME, vegetation in the Winterswijk area was dominated by the thermophilic cheirolepid conifer that produced *Classopollis* spp. Fluctuations in *Classopollis* dominance within the Contorta Beds indicate periodic shifts towards cool/warm temperate conditions (Rees *et al.* 2000), still dominated by conifers. During the Late Triassic and Early Jurassic, five distinct biomes dominated by upper canopy conifer vegetation (Willis and McElwain, 2014) have been recorded. Within the European continent, two of these biomes dominated the landscape, which includes cool/warm temperate for higher latitudes separated by a climate gradient of narrow bands of winter-wet biomes to the south (Rees *et al.* 2000). Northward migrations of winter-wet biomes (*Classopollis*-dominated) as a result of changing climatic conditions are likely the main cause for changes in plant assemblage in the Contorta Beds of the Winterswijk core (Kent and Olsen, 2000; Rees *et al.* 2000; Sellwood and Valdes, 2006). These repeated northward/southward migrations in climate gradients are caused by (orbitally paced) changes in the regional hydrological regime, which limits and enhances moisture availability (Hollaar *et al.* 2021; Bos *et al.* 2023).

Elemental compositions indicate overall wet conditions during the deposition of the Contorta Beds (low Sr/Ba and Sr/Cu ratios) with minimal terrestrial input (low Ti/Al ratio) (Fig. 5). Increases in terrestrial input, as indicated by increases in the Ti/Al ratio, suggests more efficient riverine runoff due to increased overall precipitation. Contemporary increases in aquatic palynomorphs further suggest that this could have had a significant impact on marine productivity with indications of decreased oxygen levels as evidenced by redox-sensitive elements (V/Cr and Ni/Co). The semi-enclosed nature of the CEB likely made this shallow marine/coastal setting much more sensitive to changes in the hydrological cycle and prone to water-column stratification, anoxia and algal blooms. This was in some ways similar to the volcanogenic-induced Ocean Anoxic Events during the Toarcian and Cretaceous (Hesselbo *et al.* 2000; Jenkyns, 2003; Mailliot *et al.* 2009; van de Schootbrugge *et al.* 2013; Slater *et al.* 2019). Although the main pulses of CAMP are assumed to be restricted to the Marshi and Spelae CIEs, early onset of CAMP volcanism occurred some hundred thousand years earlier and could have led to an early onset of atmospheric CO_2 increase contemporaneous with the onset of black shale deposition of the Contorta Beds.

The Triletes Beds mark a dramatic shift in paleoceanographic and paleoclimatic conditions that is evident in many proxy records presented here. It is marked by a major drop in TOC, a decrease in the absolute amounts of palynomorphs and a semi-quantitative decrease in pollen, all suggestive of a collapse in standing arborescent vegetation. This phase of forest dieback and terrestrial mass rarity has been noted in many other sections across the European continent and marks the initiation of the main extinction phase (Lindström, 2021). Whereas the proliferation of fern and fern allies during the main disturbance interval would suggest climate shifted towards more humid conditions, increases in Sr/Ba and Sr/Cu ratios seem to indicate drier conditions. However, the relatively elevated input of Sr during deposition of the clay-rich Triletes Beds could also point to more intense weathering and erosion. This is substantiated by higher abundances of reworked palynomorphs in the Triletes Beds. The resulting open landscape was likely highly susceptible to erosion and terrestrial runoff (van de Schootbrugge *et al.* 2020).

Diversity indices (dominance, evenness and Shannon-Wiener diversity) are commonly used in palaeo-ecological research to trace ecological disturbances (Svensson *et al.* 2012). Ecosystem restructuring introduces successional stages of pioneering species in a stressed ecological community leading to high evenness, diversity and low dominance (Grim, 1973; Osman, 1977; Gravendyck *et al.* 2020). Within the Contorta Beds, peaks in dominance correspond to low evenness and diversity (Shannon-Wiener and richness; Fig. 7) and are largely attributable to high abundances of *Classopollis* sp. (Fig. 8). Increased conifer (*Classopollis*) dominance is accompanied by low evenness and diversity, which suggest stable biomes without any indication of

https://doi.org/10.1017/S0016756824000323

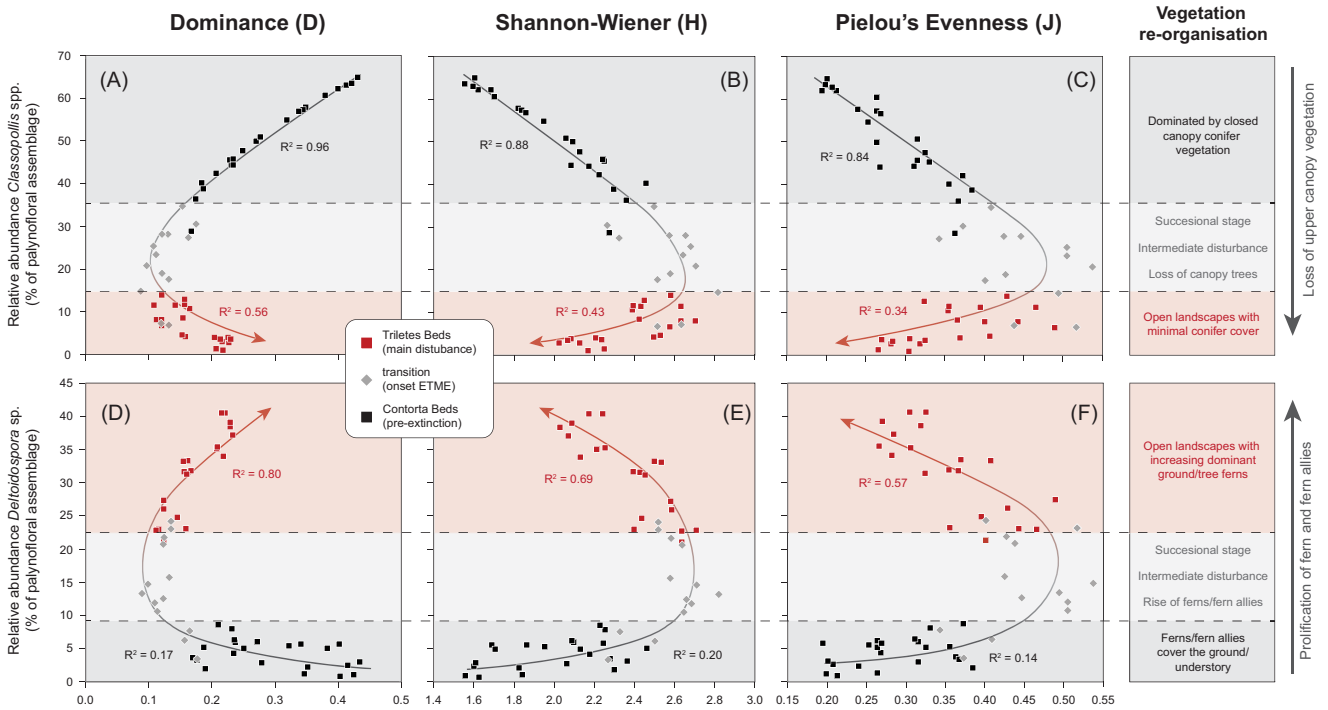

Figure 8. Correlation of palynofloral diversity indices (dominance, Shannon-Wiener diversity and evenness) and relative abundance of (upper panels) *Classopollis* sp. and (lower panels) *Deltoidospora* sp. Arrows represent progression of end-Triassic mass-extinction from Contorta Beds (black squares) to onset of extinction (grey diamonds) to Triletes Beds (red squares). Linear regression coefficient between the diversity indices and *Classopollis*/*Deltoidospora* is presented for the Contorta and Triletes Beds.

disturbance (Fig. 7). The opposite relation is noted for the intervals in between conifer dominance and seems to suggest some form of biome reorganization that is likely attributable to changes in climate conditions and/or vegetation gradients. However, no significant changes in the biome assemblages are noted within the parent vegetation groups (Fig. 7) suggesting changes in the Contorta Beds are part of the natural (orbitally-forced) climate variability. Two periods of this *Classopollis*-dominance coincide with increased abundances of aquatic palynomorphs (RLi-a (~14%) and RLi-c (~12%) subzones) suggesting marine transgressions. Sea-level variations constitute a first-order control on the preservation of organic matter and potentially could have played a role in the preferential preservation of wind-dispersed conifer pollen further from the palaeo-shoreline (the Neves effect; Chaloner (1958)). However, the lowermost samples (24.07 – 23.985 mbs; RLi-a zone) that indicate palynofloral disturbance seem unique with indication of high terrestrial input (high Ti/Al) and low TOC, hinting at a disturbed biome.

Diversity indices show a trend towards disturbed conditions (increased evenness and diversity) starting within the RLi-c subzone (T1), which is synonymous with the Marshi CIE. This shift is accompanied by a rapid increase in spore-bearing vegetation (Fig. 7) that peaks in the T2 interval (~75%). Evenness and Shannon-Wiener diversity peak within the T3 interval suggesting the presence of a successional stage and biome reorganization at this interval. Interestingly, the peaks in diversity indices see a short-lived return of pollen-bearing taxa (*Classopollis* sp. and *Ricciisporites tuberculates*). This could, however, be a side effect of a transgression within the T3 interval as noted by a sudden short-lived influx of aquatic palynomorphs, mostly dinoflagellate cysts (*R. rhaetica* and *D. priscum*). The presence of a late Rhaetian transgression in the CEB has been recorded in previous studies following the Marshi CIE (Lindström, 2016; Lindström *et al.* 2017; Lindström *et al.* 2019; Bos *et al.* 2023). This shift is accompanied by a stepwise rise in spore-bearing plants (ferns and fern allies) with tree/ground ferns (Pteridopsida/Filicopsida) becoming the dominant parent plant group, although not as significant as *Classopollis*-producing conifers in the Contorta Beds. During the deposition of the Triletes Beds, tree and ground ferns belonging to the family of Pteridopsida/Filicopsida (*Deltoidospora* sp.) indicate a good correlation with diversity indices (Fig. 8), suggesting this type of biome thrived during the main disturbance interval of the ETME.

5. c. Implications for volcanic kill mechanisms

Contrasting climate conditions between the Contorta and Triletes Beds are most likely reflective of a major swing in the hydrological regime. Palynological records from St. Audrie's Bay indicate periodic changes in terrestrial palynomorph concentrations and spore abundances during the main disturbance interval reflecting changes in monsoonal activity mediated by the 23-kyr precession cycle (Bonis *et al.* 2010). Other indicators for increased humidity are derived from elevated levels of kaolinite in boundary beds indicating enhanced chemical weathering in the North German Basin (van de Schootbrugge *et al.* 2009) and other European sections (Ahlberg *et al.* 2003; Pieńkowski *et al.* 2014; Zajzon *et al.* 2018). Alternatively, elevated kaolinite could indicate increased erosion and redeposition. Sudden shifts in atmospheric pCO_2 would also result in brief periods of regional droughts increasing the likelihood of wildfires. Major climatic perturbations in the geological past have been linked to periods of enhanced levels of wildfire activity (Baker, 2022) with several T-J boundary sections showing increased abundances of charcoal in Greenland (Belcher

https://doi.org/10.1017/S0016756824000323

et al. 2010; Williford *et al.* 2014) and Germany (Uhl and Montenari, 2011). Additionally, the Late Triassic climate conditions may have favoured combustion-prone, narrow-leaved vegetation due to increased atmospheric CO_2 levels (Belcher *et al.* 2010), which was subsequently exacerbated by widespread droughts (Peyser and Poulsen, 2008; Slodownik *et al.* 2021). The sudden dieback (mass rarity) in conifer vegetation in the Winterswijk core could be the result of enhanced wildfire activity. The resulting open landscapes were subsequently perfect for fern colonization, which fared much better during periods of enhanced monsoonal activity. Combined with instable soils, as indicated by increased reworked palynomorphs, this prevented the re-establishment of conifer tree vegetation.

Rapid and major climate shifts during the late Rhaetian and early Hettangian are thought to indicate pulses in CAMP eruptions leading to rapid large igneous province (LIP) emplacement, and the release of large quantities of volatiles (Knight *et al.* 2004). The release of CO_2 is thought to be recorded in the Marshi and Spelae CIEs across the Triassic-Jurassic boundary (Hesselbo *et al.* 2002). However, several studies have pointed to the role of strongly fluctuating carbon sources related to changes in marine versus terrestrial organic matter and changes in standing biomass. Recent studies have suggested that negative excursions in carbon isotope records could be due to shifts in organic matter source rather than volcanic injection of light ^{12}C in the atmosphere (Fox *et al.* 2020; Beith *et al.* 2023). Therefore, characterization of the sedimentary organic matter is crucial to understand the nature of the carbon cycle perturbations (Ruhl *et al.* 2010b). The Winterswijk core clearly demonstrates a severe impact on the terrestrial vegetation, mainly upper canopy conifers, during the transition from pre-extinction to extinction conditions, which is initiated at the Marshi CIE. Therefore, we can infer that the negative excursions can be partly explained through the loading of light ^{12}C from a volcanic source.

The cyclic variation of the pre-extinction (Contorta Beds) interval indicates an already turbulent climate that likely responded to variation in orbital parameters. Combined with high dominance of thermophilic cheirolepid conifers (*Classopollis*), this could indicate elevated atmospheric pCO_2 due to volcanic emissions. Furthermore, the onset of the ETME is clearly defined in both the Bonenburg and Winterswijk sections by another short-lived increase in *R. tuberculatus* corresponding to a negative CIE that has been correlated with the Marshi CIE. A similar increase in *R. tuberculatus* can be traced to other contemporaneous sections in Europe, which include the Schandelah-1 core of northern Germany (Bos *et al.* 2023), Mingolsheim core in southern Germany (van de Schootbrugge *et al.* 2009) and the Stenlille cores in Denmark (Lindström *et al.* 2023). In most cases, the increased abundance of *R. tuberculatus* persisted into the subsequent palynofloral stage. Some studies have implicated that *R. tuberculatus* is an aberrant palynomorph produced by the Peltaspermales seed plant *Lepidopteris ottonis* (Vajda *et al.* 2023; Vajda *et al.* 2024), although uncertainties remain (Zavialova, 2024). If *R. tuberculatus* is indeed an aberrant palynofloral expression, this could indicate atmospheric pollution, which further suggests a volcanic influence on the carbon isotope signature at the Marshi CIE.

The emission of volcanic pollutants can further destabilize terrestrial ecosystems. Besides direct input of greenhouse gasses, CAMP emissions included pollutants such as halocarbons (CH_3Br and CH_3Cl), potentially depleting stratospheric ozone and increasing UV-B radiation at the Earth's surface (Benca *et al.* 2018). Widespread mutagenesis has been observed in the form of aberrant pollen such as unseparated Isotelus-tetrads (*Kraeuselisporites*), attributed to elevated UV-B radiation, which either produced sterility or the capacity to reproduce asexually (Visscher *et al.* 2004; Benca *et al.* 2018; Vajda *et al.* 2023). In addition, the appearance of abnormal trisaccate pollen similarly indicates increased mutations in Permo-Triassic boundary sections as observed in Russia and China (Visscher *et al.* 2004; Foster and Afonin, 2005; Metcalfe *et al.* 2009). Intervals of elevated ozone deterioration due to volcanic pollution may have triggered temporary forest sterility and led to a population decline in several gymnosperm lineages rather than immediate extinction. Cessation of volcanic activity and a reduction in halocarbon emissions would lead to a rapidly recovering ozone layer (within 10 to 20 years) allowing for a rebound of surviving gymnosperm populations. However, combined with additional stress-inducing parameters such as increased wildfires and intense rain seasons, over time, modest seedling mortality and reduced germination could have culminated in the regional extirpation and/or extinction of gymnosperm lineages, as noted for the End-Permian crisis (Benca *et al.* 2018). The onset of extinction, as noted through the disappearance of conifer vegetation in the Winterswijk core, partly overlaps with the Marshi CIE, which is partly volcanic in origin. This volcanic pulse could have affected the established forest biome through UV-B radiated sterility combined with an enhanced hydrological cycle.

6. Conclusions

Sediments recovered in a new drill core taken near Winterswijk (The Netherlands) provide new insights into a number of palynofloral events associated with emphasis on the onset of the ETME and confirm and support previous observations from other TJ-boundary sections across Europe. A highly detailed palynostratigraphic framework identified two informal palynofloral assemblage zones (RLi and RiP zones), which provide conclusive evidence for the presence of the ETME in the Winterswijk section (Sleen Formation). By correlation with other European TJ-boundary sections, it can be shown that gradual transition through successional stages characterized the onset of the extinction. The pre-extinction interval (RLi zone) is characterized by Cheirolepidiaceae-dominated conifer forest (*Classopollis* spp.) with a notable presence of the gymnosperm *R. tuberculatus*. The transition to the main disturbance interval is noted by a successional stage that sees increased abundances of Pteridopsid ferns (*Deltoidospora* ssp.), with vegetation that overall is characterized by a shrubbier and more herbaceous cycad/fern vegetation, while upper canopy vegetation decreases. The timing of vegetational changes, leading into the main biotic crisis, confirms the recorded supra-regional structure of the ETME. Interpretations of the depositional environment, based on lithological and elemental composition, indicate overall wet climate conditions during laminated clay deposition that are synonymous with pre-extinction conditions (Contorta Beds). A transition to red claystone-dominated facies (Triletes Beds) marks the onset of the ETME and displays overall drier climate conditions. Three distinct influxes of aquatic palynomorphs further indicate marine ingressions in the Winterswijk section consistent with published reconstructions of distinct relative sea-level changes in the CEB. Furthermore, increased siliciclastic content and elevated MS intensity in the Triletes Beds, indicates riverine influx variability and confirms changes in the weathering

https://doi.org/10.1017/S0016756824000323

regime during the extinction interval. Elevated abundances in reworked palynomorphs in the Triletes Beds further suggest increased erosion rates during the main extinction interval. Indicators of aridification and increased weathering suggest major swings in the hydrological cycle. Global warming likely affected the regional climate and caused a rapid gradual decline in arborescent tree vegetation, likely through frequent wildfires and perhaps via increased UV-B radiation due to ozone depletion. Although the Winterswijk core only covers a partial record of the Late Rhaetian extinction, the succession provides a connecting site between eastern and western margins of the CEB.

Supplementary material. For supplementary material accompanying this paper visit https://doi.org/10.1017/S0016756824000323

Acknowledgements. We thank Thijssen B.V. Drilling company for conducting the scientific drilling operation at Winterswijk, for their efforts in core recovery and for providing us with the material and data studied in this report. In addition, we want to thank Sibelco B.V. for granting us access to the Winterswijk Quarry and the drilling site. Special thanks to Gerard ten Dolle for his assistance and guidance during the drilling operation and for providing the team with adequate background information regarding the geological subsurface of the surrounding area. We are grateful for the technical support at Utrecht University by Maxim Krasnoperov, Desmond Eefting, Arnold van Dijk, Giovanni Dammers and Natasja Welters.

Author contributions. The project was designed by RB and BvdS. Core retrieval was managed by RB, RJvZ, JR, GJV and NJ. Core description was conducted by RB, RJvZ and NJ. Laboratory analysis was performed by RB with assistance from TE. Palynomorph specimen identification and documentation were undertaken by RB with assistance from BvdS. Data analyses and visualization were carried out by RB. RB wrote the paper with input from all authors.

Competing interests. The authors declare that they have no competing interests.

Financial statement. This study was funded through the Dutch Research Council open programme (NWO ALWOP.623) to whom we are grateful for providing us with the opportunity to conduct this research.

References

Ahlberg A, Olsson I and Šimkevičius P (2003) Triassic–Jurassic weathering and clay mineral dispersal in basement areas and sedimentary basins of southern Sweden. *Sedimentary Geology* **161**(1-2), 15–29.

Bai Y, Liu Z, Sun P, Liu R, Hu X, Zhao H and Xu Y (2015) Rare earth and major element geochemistry of Eocene fine-grained sediments in oil shale- and coal-bearing layers of the Meihe Basin, Northeast China. *Journal of Asian Earth Sciences* **97**, 89–101.

Baker SJ (2022) Fossil evidence that increased wildfire activity occurs in tandem with periods of global warming in Earth's past. *Earth-Science Reviews* **224**, 103871.

Barbacka M, Pacyna G, Kocsis ÁT, Jarzynka A, Ziaja J and Bodor E (2017) Changes in terrestrial floras at the Triassic-Jurassic Boundary in Europe. *Palaeogeography, Palaeoclimatology, Palaeoecology* **480**, 80–93.

Beerling DJ and Berner RA (2002) Biogeochemical constraints on the Triassic-Jurassic boundary carbon cycle event. *Global Biogeochemical Cycles* **16**(3), 10-1-10-13.

Beith SJ, Fox CP, Marshall JE and Whiteside JH (2023) Compound-specific carbon isotope evidence that the initial carbon isotope excursion in the end-Triassic strata in northwest Tethys is not the product of CAMP magmatism. *Global and Planetary Change* **222**, 104044.

Belcher CM, Mander L, Rein G, Jervis FX, Haworth M, Hesselbo SP, Glasspool IJ and McElwain JC (2010) Increased fire activity at the Triassic/Jurassic boundary in Greenland due to climate-driven floral change. *Nature Geoscience* **3**(6), 426–29.

Benca JP, Duijnstee IA and Looy CV (2018) UV-B–induced forest sterility: Implications of ozone shield failure in Earth's largest extinction. *Science Advances* **4**(2), e1700618.

Blackburn TJ, Olsen PE, Bowring SA, McLean NM, Kent DV, Puffer J, McHone G, Rasbury ET and Et-Touhami M (2013) Zircon U-Pb geochronology links the end-Triassic extinction with the Central Atlantic Magmatic Province. *Science* **340**(6135), 941–45.

Blakey RC (2014) Paleogeography and paleotectonics of the western interior seaway, Jurassic-Cretaceous of North America. *Search and Discovery* **30392**, 72.

Bonis NR and Kürschner WM (2012) Vegetation history, diversity patterns, and climate change across the Triassic/Jurassic boundary. *Paleobiology* **38**(2), 240–64.

Bonis NR, Kürschner WM and Krystyn L (2009) A detailed palynological study of the Triassic–Jurassic transition in key sections of the Eiberg Basin (Northern Calcareous Alps, Austria). *Review of Palaeobotany and Palynology* **156**(3-4), 376–400.

Bonis NR, Ruhl M and Kürschner WM (2010) Climate change driven black shale deposition during the end-Triassic in the western Tethys. *Palaeogeography, Palaeoclimatology, Palaeoecology* **290**(1-4), 151–59.

Borrok DM, Yang W, Wei M and Mokhtari M (2019) Heterogeneity of the mineralogy and organic content of the Tuscaloosa Marine Shale. *Marine and Petroleum Geology* **109**, 717–31.

Bos R, Lindström S, van Konijnenburg-van Cittert H, Hilgen F, Hollaar TP, Aalpoel H, van der Weijst C, Sanei H, Rudra A, Sluijs A and van de Schootbrugge B (2023) Triassic-Jurassic vegetation response to carbon cycle perturbations and climate change. *Global and Planetary Change* **228**, 104211.

Bos R, Zheng W, Lindström S, Sanei H, Waajen I, Fendley I, Mather T, Wang Y, Rohovec J, Navrátil T, Sluijs A and van de Schootbrugge, B (2024) Climate-forced Hg-remobilization associated with fern mutagenesis in the aftermath of the end-Triassic extinction. *Nature Communications* **15**, 3596.

Brugman W, Eggink J and Visscher H (1985) Middle Triassic (Anisian-Ladinian) Palynomorphs. *Journal of Micropalaeontolgy* **4**(1), 107–11.

Capriolo M, Mills BJ, Newton RJ, Dal Corso J, Dunhill AM, Wignall PB and Marzoli A (2022). Anthropogenic-scale CO2 degassing from the Central Atlantic Magmatic Province as a driver of the end-Triassic mass extinction. *Global and Planetary Change* **209**, 103731.

Caroff M and Cotten J (2004) Geochemical evolution of a 10 m-thick intrusive body: the South Brenterc'h diabase dyke, Western Armorican Massif, France. *Canadian Journal of Earth Sciences* **41**(7), 775–84.

Chaloner WG (1958) The Carboniferous Upland Flora. *Geological Magazine* **95**(3), 261–62.

Chen H-F, Yeh P-Y, Song S-R, Hsu S-C, Yang T-N, Wang Y, Chi Z, Lee T-Q, Chen M-T and Cheng C-L (2013) The Ti/Al molar ratio as a new proxy for tracing sediment transportation processes and its application in aeolian events and sea level change in East Asia. *Journal of Asian Earth Sciences* **73**, 31–38.

Corso JD, Marzoli A, Tateo F, Jenkyns HC, Bertrand H, Youbi N, Mahmoudi A, Font E, Buratti N and Cirilli S (2014) The dawn of CAMP volcanism and its bearing on the end-Triassic carbon cycle disruption. *Journal of the Geological Society* **171**(2), 153–64.

de Lange B, Chenal E, Diependaal HJ and Reumer JW (2023) Fish remains from the Rhaetian (Late Triassic) of Winterswijk, the Netherlands (Pisces: Chondrichthyes and Actinopterygii). Netherlands. *Journal of Geosciences* **102**, e10.

Deenen MHL, Ruhl M, Bonis NR, Krijgsman W, Kuerschner WM, Reitsma M and van Bergen MJ (2010). A new chronology for the end-Triassic mass extinction. *Earth and Planetary Science Letters* **291**(1-4), 113–25.

Doornenbal H and Stevenson A (2010) *Petroleum geological atlas of the Southern Permian Basin area*. EAGE.

Foster C and Afonin S (2005) Abnormal pollen grains: an outcome of deteriorating atmospheric conditions around the Permian–Triassic boundary. *Journal of the Geological Society* **162**(4), 653–59.

Fowell S and Olsen P (1993) Time calibration of Triassic/Jurassic microfloral turnover, eastern North America. *Tectonophysics* **222**(3-4), 361–69.

Fox CP, Cui X, Whiteside JH, Olsen PE, Summons RE and Grice K (2020) Molecular and isotopic evidence reveals the end-Triassic carbon isotope

excursion is not from massive exogenous light carbon. *Proceedings of the National Academy of Sciences* **117**(48), 30171–78.

Fu X, Wang J, Chen W, Feng X, Wang D, Song C and Zeng S (2016) Elemental geochemistry of the early Jurassic black shales in the Qiangtang Basin, eastern Tethys: constraints for palaeoenvironment conditions. *Geological Journal* **51**(3), 443–54.

Golonka J, Embry A and Krobicki M (2018) Late triassic global plate tectonics. In *The Late Triassic World*. 27–57. Cham: Springer.

Götz A, Ruckwied K, Pálfy J and Haas J (2009) Palynological evidence of synchronous changes within the terrestrial and marine realm at the Triassic/Jurassic boundary (Csővár section, Hungary). *Review of Palaeobotany and Palynology* **156**(3-4), 401–09.

Gravendyck J, Schobben M, Bachelier JB and Kürschner WM (2020) Macroecological patterns of the terrestrial vegetation history during the end-Triassic biotic crisis in the central European Basin: A palynological study of the Bonenburg section (NW-Germany) and its supra-regional implications. *Global and Planetary Change* **194**, 103286.

Grim JP (1973) Competition and diversity in herbaceous vegetation (reply). *Nature* **244**(5414), 311.

Hammer Ø, Harper DA and Ryan PD (2001) PAST: Paleontological statistics software package for education and data analysis. *Palaeontologia Electronica* **4**(1), 9.

Harsveldt H (1973) The middle triassic limestone (Muschelkalk) in the Achterhoek (E. Gelderland). In *New Aspects of Mineral and Water Resources in The Netherlands*, pp. 43–49. Dordrecht: Springer.

Heimdal TH, Svensen HH, Ramezani J, Iyer K, Pereira E, Rodrigues R, Jones MT and Callegaro S (2018) Large-scale sill emplacement in Brazil as a trigger for the end-Triassic crisis. *Scientific Reports* **8**(1), 1–12.

Herngreen G, Van Konijnenburg-van Cittert J and Oosterink H (2005) New geological data (Middle Triassic, Rhaetian-Liassic and Oligocene) of the Winterswijk quarry, the eastern Netherlands. Netherlands. *Journal of Geosciences* **84**(4), 409–13.

Hesselbo SP, Al-Suwaidi A, Baker SJ, Ballabio G, Belcher CM, Bond A, Boomer I, Bos R, Bjerrum CJ, Boyle R, Browning JV, Butcher, AR, Condon, DJ, Copestake, P, Daines, S, Dalby, C, Damaschke, M, Damborenea, SE, Deconinck, JF, Dickson, AJ, Fendley IM, Fox CP, Fraguas A, Frieling J, Gibson TA, He T, Hickey K, Hinnov LA, Hollaar TP, Huang C, Hudson AJL, Jenkyns HC, Idiz E, Jiang M, Krijgsman W, Korte C, Leng MJ, Lenton TM, Leu K, Little CTS, MacNiocaill C, Manceñido MO, Mather TA, Mattioli E, Miller KG, Newton RJ, Page KN, Pálfy J, Pieńkowski G, Porter RJ, Poulton SW, Riccardi AC, Riding JB, Roper A, Ruhl M, Silva RL, Storm MS, Suan G, Szűcs D, Thibault N, Uchman A, Stanley JN, Ullmann CV, van de Schootbrugge B, Vickers ML, Wadas S, Whiteside JH, Wignall PB, Wonik T, Xu W, Zeeden C and Zhao K (2023) Initial results of coring at Prees, Cheshire Basin, UK (ICDP JET project): towards an integrated stratigraphy, timescale, and Earth system understanding for the Early Jurassic. *Scientific Drilling* **32**, 1–25.

Hesselbo SP, Gröcke DR, Jenkyns HC, Bjerrum CJ, Farrimond P, Morgans Bell HS and Green OR (2000) Massive dissociation of gas hydrate during a Jurassic oceanic anoxic event. *Nature* **406**(6794), 392–95.

Hesselbo SP, Robinson SA, Surlyk F and Piasecki S (2002) Terrestrial and marine extinction at the Triassic-Jurassic boundary synchronized with major carbon-cycle perturbation: A link to initiation of massive volcanism? *Geology* **30**(3), 251–54.

Heunisch C, Luppold FW, Reinhardt L and Röhling H-G (2010) Palynofazies, bio-und Lithostratigrafie im grenzbereich Trias/Jura in der bohrung Mariental 1 (Lappwaldmulde, Ostniedersachsen). *Zeitschrift der Deutschen Gesellschaft für Geowissenschaften*, **161**, 51–98.

Hollaar TP, Baker SJ, Hesselbo SP, Deconinck J-F, Mander L, Ruhl M and Belcher CM (2021) Wildfire activity enhanced during phases of maximum orbital eccentricity and precessional forcing in the Early Jurassic. *Communications Earth & Environment* **2**(1), 1–12.

Huynh TT and Poulsen CJ (2005) Rising atmospheric CO2 as a possible trigger for the end-Triassic mass extinction. *Palaeogeography, Palaeoclimatology, Palaeoecology* **217**(3-4), 223–42.

Jenkyns HC (2003) Evidence for rapid climate change in the Mesozoic–Palaeogene greenhouse world. *Philosophical Transactions of the Royal Society of London. Series A: Mathematical, Physical and Engineering Sciences* **361**(1810), 1885–916.

Kent DV and Olsen PE (2000) Magnetic polarity stratigraphy and paleolatitude of the Triassic-Jurassic Blomidon Formation in the Fundy basin (Canada): implications for early Mesozoic tropical climate gradients. *Earth and Planetary Science Letters* **179**, 311–24.

Knight KB, Nomade S, Renne PR, Marzoli A, Bertrand H and Youbi N (2004) The Central Atlantic Magmatic Province at the Triassic–Jurassic boundary: paleomagnetic and 40Ar/39Ar evidence from Morocco for brief, episodic volcanism. *Earth and Planetary Science Letters* **228**(1-2), 143–60.

Kovács EB, Ruhl M, Demény A, Fórizs I, Hegyi I, Horváth-Kostka ZR, Móricz F, Vallner Z and Pálfy J (2020) Mercury anomalies and carbon isotope excursions in the western Tethyan Csővár section support the link between CAMP volcanism and the end-Triassic extinction. *Global and Planetary Change* **194**, 103291.

Kuerschner WM, Bonis NR and Krystyn L (2007) Carbon-isotope stratigraphy and palynostratigraphy of the Triassic–Jurassic transition in the Tiefengraben section — Northern Calcareous Alps (Austria). *Palaeogeography, Palaeoclimatology, Palaeoecology* **244**(1-4), 257–80.

Landwehrs J, Feulner G, Willeit M, Petri S, Sames B, Wagreich M, Whiteside JH and Olsen PE (2022) Modes of Pangean lake level cyclicity driven by astronomical climate pacing modulated by continental position and pCO[Formula: see text]. *Proceedings of the National Academy of Sciences of the United States of America* **119**(46), e2203818119.

Landwehrs JP, Feulner G, Hofmann M and Petri S (2020) Climatic fluctuations modeled for carbon and sulfur emissions from end-Triassic volcanism. *Earth and Planetary Science Letters* **537**, 116174.

Larsson LM (2009) Palynostratigraphy of the Triassic–Jurassic transition in southern Sweden. *GFF* **131**(1-2), 147–63.

Li L, Wang Y, Liu Z, Zhou N and Wang Y (2016) Late Triassic palaeoclimate and palaeoecosystem variations inferred by palynological record in the northeastern Sichuan Basin, China. *Paläontologische Zeitschrift* **90**(2), 327–48.

Lindström S (2016) Palynofloral patterns of terrestrial ecosystem change during the end-Triassic event – a review. *Geological Magazine* **153**(2), 223–51.

Lindström, S. (2021) Two-phased Mass Rarity and Extinction in Land Plants During the End-Triassic Climate Crisis. *Frontiers in Earth Science* **9**(9), 1079.

Lindström S, Callegaro S, Davies J, Tegner C, van de Schootbrugge B, Pedersen GK, Youbi N, Sanei H and Marzoli A (2021) Tracing volcanic emissions from the Central Atlantic Magmatic Province in the sedimentary record. *Earth-Science Reviews* **212**, 103444.

Lindström S, Pedersen GK, Vosgerau H, Hovikoski J, Dybkjaer K and Nielsen LH (2023) Palynology of the Triassic–Jurassic transition of the Danish Basin (Denmark): a palynostratigraphic zonation of the Gassum–lower Fjerritslev formations. *Palynology* **47**(4), 2241068.

Lindström S, Sanei H, Van De Schootbrugge B, Pedersen GK, Lesher CE, Tegner C, Heunisch C, Dybkjær K and Outridge PM (2019) Volcanic mercury and mutagenesis in land plants during the end-Triassic mass extinction. *Science Advances* **5**(10), eaaw4018.

Lindström S, van de Schootbrugge B, Dybkjaer K, Pedersen GK, Fiebig J, Nielsen LH and Richoz S (2012) No causal link between terrestrial ecosystem change and methane release during the end-Triassic mass extinction. *Geology* **40**(6), 531–34.

Lindström S, van de Schootbrugge B, Hansen KH, Pedersen GK, Alsen P, Thibault N, Dybkjær K, Bjerrum CJ and Nielsen LH (2017) A new correlation of Triassic–Jurassic boundary successions in NW Europe, Nevada and Peru, and the Central Atlantic Magmatic Province: A time-line for the end-Triassic mass extinction. *Palaeogeography, Palaeoclimatology, Palaeoecology* **478**, 80–102.

Lund J (2003) Rhaetian to Pliensbachian palynostratigraphy of the central part of the NW German Basin exemplified by the Eitzendorf 8 well. *Courier-Forschungsinstitut Senckenberg*, **241**, 69–84.

Lund JJ (1977) Rhaetic to Lower Liassic palynology of the onshore south-eastern North Sea Basin. *Danmarks Geologiske Undersøgelse II. Række* **109**, 1–128.

Mailliot S, Mattioli E, Bartolini A, Baudin F, Pittet B and Guex J (2009) Late Pliensbachian–Early Toarcian (Early Jurassic) environmental changes in an epicontinental basin of NW Europe (Causses area, central France): A

micropaleontological and geochemical approach. *Palaeogeography, Palaeoclimatology, Palaeoecology* **273**(3-4), 346–64.

Mander L (2011) Taxonomic resolution of the Triassic–Jurassic sporomorph record in East Greenland. *Journal of Micropalaeontology* **30**(2), 107–18.

Mander L, Kürschner WM and McElwain JC (2013) Palynostratigraphy and vegetation history of the Triassic–Jurassic transition in East Greenland. *Journal of the Geological Society* **170**(1), 37–46.

Manspeizer W (1994) The breakup of Pangea and its impact on climate: consequences of Variscan±Alleghanide orogenic collapse. *Geological Society of America Special Papers* **288**, 169–85.

McElwain JC, Beerling DJ and Woodward FI (1999) Fossil plants and global warming at the Triassic-Jurassic boundary. *Science* **285**(5432), 1386–90.

McGhee GR, Clapham ME, Sheehan PM, Bottjer DJ and Droser ML (2013) A new ecological-severity ranking of major Phanerozoic biodiversity crises. *Palaeogeography, Palaeoclimatology, Palaeoecology* **370**, 260–70.

Meng Q, Liu Z, Bruch AA, Liu R and Hu F (2012) Palaeoclimatic evolution during Eocene and its influence on oil shale mineralisation, Fushun basin, China. *Journal of Asian Earth Sciences* **45**, 95–105.

Metcalfe I, Foster C, Afonin S, Nicoll R, Mundil R, Xiaofeng W and Lucas S (2009) Stratigraphy, biostratigraphy and C-isotopes of the Permian–Triassic non-marine sequence at Dalongkou and Lucaogou, Xinjiang Province, China. *Journal of Asian Earth Sciences* **36**(6), 503–20.

Moradi AV, Sarı A and Akkaya P (2016) Geochemistry of the Miocene oil shale (Hançili Formation) in the Çankırı-Çorum Basin, Central Turkey: Implications for Paleoclimate conditions, source–area weathering, provenance and tectonic setting. *Sedimentary Geology* **341**, 289–303.

Olsen PE, Koeberl C, Huber H, Montanari A, Fowell SJ, Et-Touhami M and Kent DV (2002) Continental Triassic-Jurassic boundary in central Pangea: Recent progress and discussion of an Ir anomaly.

Osman RW (1977) The establishment and development of a marine epifaunal community. *Ecological Monographs* **47**(1), 37–63.

Peng J, Li J, Li W, Slater SM, Zhu H and Vajda V (2018) The Triassic to Early Jurassic palynological record of the Tarim Basin, China. *Palaeobiodiversity and Palaeoenvironments* **98**(1), 7–28.

Percival LM, Bergquist BA, Mather TA and Sanei H (2021) Sedimentary mercury enrichments as a tracer of large igneous province volcanism. In *Large Igneous Provinces: A Driver of Global Environmental And Biotic Changes* (eds RE Ernst, AJ Dickson and A Bekker) pp. 247–62, Hoboken, USA: John Wiley and Sons, Inc.

Percival LME, Ruhl M, Hesselbo SP, Jenkyns HC, Mather TA and Whiteside JH (2017) Mercury evidence for pulsed volcanism during the end-Triassic mass extinction. *Proceedings of the National Academy of Sciences of the United States of America* **114**(30), 7929–34.

Peyser CE and Poulsen CJ (2008) Controls on Permo-Carboniferous precipitation over tropical Pangaea: A GCM sensitivity study. *Palaeogeography, Palaeoclimatology, Palaeoecology* **268**(3-4), 181–92.

Pieńkowski G, Niedźwiedzki G and Brański P (2014) Climatic reversals related to the Central Atlantic magmatic province caused the end-Triassic biotic crisis—Evidence from continental strata in Poland. Volcanism, Impacts, and Mass Extinctions: Causes and Effects. *Geological Society of America Special Papers* **505**, 263–86.

Pieńkowski G, Niedźwiedzki G and Waksmundzka M (2012) Sedimentological, palynological and geochemical studies of the terrestrial Triassic–Jurassic boundary in northwestern Poland. *Geological Magazine* **149**(2), 308–32.

Rees PM, Ziegler AM, Valdes PJ, Huber BT, Macleod KG and Wing SL (2000) Jurassic phytogeography and climates: new data and model comparisons. *Warm Climates in Earth History*. **110**, 297–318.

Rimmer SM (2004) Geochemical paleoredox indicators in Devonian–Mississippian black shales, central Appalachian Basin (USA). *Chemical Geology* **206**(3-4), 373–91.

Ruckwied K, Götz AE, Pálfy J and Török Á (2008) Palynology of a terrestrial coal-bearing series across the Triassic/Jurassic boundary (Mecsek Mts, Hungary). *Central European Geology* **51**(1), 1–15.

Ruhl M, Deenen MHL, Abels HA, Bonis NR, Krijgsman W and Kürschner WM (2010a) Astronomical constraints on the duration of the early Jurassic Hettangian stage and recovery rates following the end-Triassic mass extinction (St Audrie's Bay/East Quantoxhead, UK). *Earth and Planetary Science Letters* **295**(1-2), 262–76.

Ruhl M, Hesselbo SP, Al-Suwaidi A, Jenkyns H, Damborenea SE, Manceñido MO, Storm M, Mather T and Riccardi AC (2020) On the onset of Central Atlantic Magmatic Province (CAMP) volcanism and environmental and carbon-cycle change at the Triassic–Jurassic transition (Neuquén Basin, Argentina). *Earth-Science Reviews* **208**, 103229.

Ruhl M, Veld H and Kürschner WM (2010b) Sedimentary organic matter characterization of the Triassic–Jurassic boundary GSSP at Kuhjoch (Austria). *Earth and Planetary Science Letters* **292**(1-2), 17–26.

Schaller MF (2012) *Large igneous provinces and Earth's carbon cycle: Lessons from the Late Triassic and rapidly emplaced Central Atlantic Magmatic Province*. New Brunswick, USA: Rutgers The State University of New Jersey, School of Graduate Studies.

Schaller MF, Wright JD and Kent DV (2011) Atmospheric p CO2 perturbations associated with the Central Atlantic Magmatic Province. *Science* **331**(6023), 1404–09.

Schneebeli-Hermann E, Hochuli PA and Bucher H (2017) Palynofloral associations before and after the Permian–Triassic mass extinction, Kap Stosch, East Greenland. *Global and Planetary Change* **155**, 178–95.

Schobben M, Gravendyck J, Mangels F, Struck U, Bussert R, Kürschner WM, Korn D, Sander PM and Aberhan M (2019) A comparative study of total organic carbon-δ13C signatures in the Triassic–Jurassic transitional beds of the Central European Basin and western Tethys shelf seas. *Newsletters on Stratigraphy* **52**(4), 461–86.

Sellwood BW and Valdes PJ (2006) Mesozoic climates: General circulation models and the rock record. *Sedimentary Geology* **190**(1-4), 269–87.

Shannon CE and Weaver W (1949) The mathematical theory of information. *Urbana: University of Illinois Press* **97**(6), 128–64.

Shen J, Yin R, Algeo TJ, Svensen HH and Schoepfer SD (2022a) Mercury evidence for combustion of organic-rich sediments during the end-Triassic crisis. *Nature Communications* **13**(1), 1307.

Shen J, Yin R, Zhang S, Algeo TJ, Bottjer DJ, Yu J, Xu G, Penman D, Wang Y, Li L, Shi X, Planavsky NJ, Feng Q and Xie S (2022b) Intensified continental chemical weathering and carbon-cycle perturbations linked to volcanism during the Triassic-Jurassic transition. *Nature Communications* **13**(1), 299.

Simpson EH (1949) Measurement of diversity. *Nature* **163**(4148), 688–.

Slater SM, Twitchett RJ, Danise S and Vajda V (2019) Substantial vegetation response to Early Jurassic global warming with impacts on oceanic anoxia. *Nature Geoscience* **12**(6), 462–67.

Slodownik M, Vajda V and Steinthorsdottir M (2021) Fossil seed fern Lepidopteris ottonis from Sweden records increasing CO2 concentration during the end-Triassic extinction event. *Palaeogeography, Palaeoclimatology, Palaeoecology* **564**, 110157.

Steinthorsdottir M, Jeram AJ and McElwain JC (2011) Extremely elevated CO2 concentrations at the Triassic/Jurassic boundary. *Palaeogeography, Palaeoclimatology, Palaeoecology* **308**(3-4), 418–32.

Svensson JR, Lindegarth M, Jonsson PR and Pavia H (2012) Disturbance-diversity models: what do they really predict and how are they tested? *Proceedings of the Royal Society B: Biological Sciences* **279**(1736), 2163–70.

Thibodeau AM, Ritterbush K, Yager JA, West AJ, Ibarra Y, Bottjer DJ, Berelson WM, Bergquist BA and Corsetti FA (2016) Mercury anomalies and the timing of biotic recovery following the end-Triassic mass extinction. *Nature Communications* **7**, 11147.

Uhl D and Montenari M (2011) Charcoal as evidence of palaeo-wildfires in the Late Triassic of SW Germany. *Geological Journal* **46**(1), 34–41.

Vajda V, McLoughlin S, Slater SM, Gustafsson O and Rasmusson AG (2023) The 'seed-fern'Lepidopteris mass-produced the abnormal pollen Ricciisporites during the end-Triassic biotic crisis. *Palaeogeography, Palaeoclimatology, Palaeoecology* **627**, 111723.

Vajda V, McLoughlin S, Slater SM, Gustafsson O and Rasmusson AG (2024) Confirmation that Antevsia zeilleri microsporangiate organs associated with latest Triassic Lepidopteris ottonis (Peltaspermales) leaves produced Cycadopites-Monosulcites-Chasmatosporites-and Ricciisporites-type monosulcate pollen. *Palaeogeography, Palaeoclimatology, Palaeoecology* **640**, 112111.

van de Schootbrugge B, Bachan A, Suan G, Richoz S and Payne JL (2013) Microbes, mud and methane: cause and consequence of recurrent Early

Jurassic anoxia following the end-Triassic mass extinction. *Palaeontology* **56**(4), 685–709.

van de Schootbrugge B, Quan TM, Lindström S, Püttmann W, Heunisch C, Pross J, Fiebig J, Petschick R, Röhling HG, Richoz S, Rosenthal Y and Falkowski PG (2009) Floral changes across the Triassic/Jurassic boundary linked to flood basalt volcanism. *Nature Geoscience* **2**(8), 589–94.

van de Schootbrugge B, van der Weijst CMH, Hollaar TP, Vecoli M, Strother PK, Kuhlmann N, Thein J, Visscher H, van Konijnenburg-van Cittert H, Schobben MAN, Sluijs, A. and Lindström S (2020) Catastrophic soil loss associated with end-Triassic deforestation. *Earth-Science Reviews* **210**, 103332.

van den Bosch M, Cadée MC and Janssen AW (1975) Lithostratigraphical and biostratigraphical subdivision of Tertiary deposits (Oligocene-Pliocene) in the Winterswijk-Almelo region (eastern part of the Netherlands). *Scripta Geologica* **29**, 1–167.

van der Meer DG, Scotese CR, Mills BJ, Sluijs A and van de Weg RM (2022) Long-term Phanerozoic global mean sea level: Insights from strontium isotope variations and estimates of continental glaciation. *Gondwana Research* **111**, 103–21.

van Hinsbergen LP, van Hinsbergen DJ, Langereis CG, Dekkers MJ, Zanderink B and Deenen MH (2019) Triassic (Anisian and Rhaetian) palaeomagnetic poles from the Germanic Basin (Winterswijk, the Netherlands). *Journal of Palaeogeography* **8**, 1–15.

van Konijnenburg-van Cittert JH, Schmeißner S, Dütsch G, Kustatscher E and Pott C (2022) Plant macrofossils from the Rhaetian of Einberg near Coburg (Bavaria, Germany). Part 2. Cycadophyta and Ginkgophyta. *Neues Jahrbuch für Geologie und Paläontologie-Abhandlungen* **305**, 109–30.

van Konijnenburg-van Cittert JHA, Pott C, Schmeißner S, Dütsch G and Kustatscher E (2020) Ferns and fern allies in the Rhaetian flora of Wüstenwelsberg, Bavaria, Germany. *Review of Palaeobotany and Palynology* **273**, 104147.

van Konijnenburg-van Cittert JHA, Pott C, Schmeißner S, Dütsch G and Kustatscher E (2021) The Rhaetian flora of Wüstenwelsberg, Bavaria, Germany: Description of selected gymnosperms (Ginkgoales, Cycadales, Coniferales) together with an ecological assessment of the locally prevailing vegetation. *Review of Palaeobotany and Palynology* **288**, 104398.

Visscher H and Commissaris A (1968) Middle Triassic pollen and spores from the Lower Muschelkalk of Winterswijk (the Netherlands). *Mededelingen van het Botanisch Museum en Herbarium van de Rijksuniversiteit te Utrecht* **307**(1), 161–76.

Visscher H, Looy CV, Collinson ME, Brinkhuis H, van Konijnenburg-van Cittert JH, Kurschner WM and Sephton MA (2004) Environmental mutagenesis during the end-Permian ecological crisis. *Proceedings of the National Academy of Sciences of the United States of America* **101**(35), 12952–6.

von Hillebrandt A and Krystyn L (2009) On the oldest Jurassic ammonites of Europe (Northern Calcareous Alps, Austria) and their global significance. *Neues Jahrbuch für Geologie und Paläontologie - Abhandlungen* **253**(2-3), 163–95.

von Hillebrandt AV, Krystyn L and Kuerschner WM (2007) A candidate GSSP for the base of the Jurassic in the Northern Calcareous Alps (Kuhjoch section, Karwendel Mountains, Tyrol, Austria). *International Subcommission on Jurassic Stratigraphy Newsletter* **34**(1), 2–20.

von Hillebrandt AV, Krystyn L, Kürschner WM, Bonis NR, Ruhl M, Richoz S, Schobben MAN, Urlichs M, Bown PR, Kment K and McRoberts CA (2013) The global stratotype sections and point (GSSP) for the base of the Jurassic System at Kuhjoch (Karwendel Mountains, Northern Calcareous Alps, Tyrol, Austria). *Episodes* **36**(3), 162–98.

Warrier AK and Shankar R (2009) Geochemical evidence for the use of magnetic susceptibility as a paleorainfall proxy in the tropics. *Chemical Geology* **265**(3-4), 553–62.

Whiteside JH, Olsen PE, Eglinton T, Brookfield ME and Sambrotto RN (2010) Compound-specific carbon isotopes from Earth's largest flood basalt eruptions directly linked to the end-Triassic mass extinction. *Proceedings of the National Academy of Sciences of the United States of America* **107**(15), 6721–5.

Wignall PB and Atkinson JW (2020) A two-phase end-Triassic mass extinction. *Earth-Science Reviews* **208**, 103282.

Williford KH, Grice K, Holman A and McElwain JC (2014) An organic record of terrestrial ecosystem collapse and recovery at the Triassic–Jurassic boundary in East Greenland. *Geochimica et Cosmochimica Acta* **127**, 251–63.

Willis K and McElwain J (2014) *The evolution of plants*. Oxford University Press.

Yager JA, West AJ, Thibodeau AM, Corsetti FA, Rigo M, Berelson WM, Bottjer DJ, Greene SE, Ibarra Y, Jadoul F, Ritterbush KA, Rollins N, Rosas S, Di Stefano P, Sulca D, Todaro S, Wynn P, Zimmermann L and Bergquist BA (2021) Mercury contents and isotope ratios from diverse depositional environments across the Triassic–Jurassic Boundary: Towards a more robust mercury proxy for large igneous province magmatism. *Earth-Science Reviews* **223**, 103775.

Zajzon N, Kristály F, Pálfy J and Németh T (2018) Detailed clay mineralogy of the Triassic-Jurassic boundary section at Kendlbachgraben (Northern Calcareous Alps, Austria). *Clay Minerals* **47**(2), 177–89.

Zavialova N (2024) Comment on "The 'seed-fern'Lepidopteris mass-produced the abnormal pollen Ricciisporites during the end-Triassic biotic crisis" by V. Vajda, S. McLoughlin, SM Slater, O. Gustafsson, and AG Rasmusson [Palaeogeography, Palaeoclimatology, Palaeoecology, 627 (2023), 111,723]. *Review of Palaeobotany and Palynology* **322**, 105065.